Interleukin-34 orchestrates bone formation through its binding to Bone Morphogenic Proteins

Dominique Heymann, Frédéric Lézot, Javier Muñoz-Garcia, Jorge William Vargas-Franco, Kristina Schiavone, Marcus T. Keatinge, Robin Young, Jérôme Amiaud, Laurie Fradet, Jean-François Jégou, et al.

Title:

Interleukin-34 orchestrates bone formation through its binding to Bone Morphogenic Proteins

Authors:

Javier Muñoz-Garcia[1,2]†, Jorge W. Vargas-Franco[3]†, Kristina Schiavone[4], Marcus T. Keatinge[5], Robin Young[6], Jérôme Amiaud[7], Laurie Fradet[1], Jean-François Jégou[8], Hideo Yagita[9], Claudine Blin-Wakkach[10], Abdelilah Wakkach[10], Denis Cochonneau[2], Emilie Ollivier[2], Martine Pugière[11], Corinne Henriquet[11], Marie Legendre[12], Irina Giurgea[12], Serge Amselem[12], Marie-Françoise Heymann[1,2], Stéphane Télétchéa[1], Frédéric Lézot[12]‡*, Dominique Heymann[1,2,4,7]‡*.

Affiliations:

[1] Nantes University, CNRS, US2B, UMR 6286, Nantes, France, 44300.

[2] Institut de Cancérologie de l'Ouest, Saint-Herblain, France, 44805.

[3] University of Antioquia, Department of Basic Studies, Faculty of Odontology, Medellin,Colombia, 1225.

[4] Université of Sheffield, School of Medicine and Population Health, Sheffield, UK, S10 2TN.

[5] University of Edinburgh, Centre for Discovery Brain Sciences, Edinburgh, UK, EH8 9XD.

[6] Sheffield Teaching Hospitals NHS Foundation Trust, Sheffield, UK, S10 2JF.

[7] Nantes University, Department of Histology and Embryology, Medical School, Nantes, France, 44000.

[8] University of Poitiers, LITEC, UR15560, Poitiers, France, 86073.

[9] Juntendo University, Department of Immunology, School of Medicine, Tokyo, Japan, 113-8421.

[10] University Côte d'Azur, CNRS, UMR7370, LP2M, Nice, France, 06107.

[11] University of Montpellier, INSERM, UMR1194, IRCM, Montpellier, France, 34298.

[12] Sorbonne University, INSERM, UMR933, Hospital Armand-Trousseau (AP-HP), Paris, France, 75012.

†,‡ These authors contributed equally to this work

***Corresponding authors:**

Dominique Heymann
Institut de Cancérologie de l'Ouest
Boulevard Professeur Jacques Monod
Saint-Herblain, France, 44805
dominique.heymann@univ-nantes.fr
00 33 (0)2 40 67 9841

Frédéric Lézot
INSERM UMR933
Hôpital Armand-Troussea
26 Avenue du Dr Arnold Netter
Paris, France, 75012
frederic.lezot@inserm.fr
00 33 (0)1 44 73 52 39

Author contributions:

Conceptualization: JM-G, JWV-F, ST, FL, DH.

Methodology: JM-G, JWV-F, KS, MTK, RY, JA, LF, J-FJ, HY, CB-W, AW, DC, EO, MP, CH, ML, IG, SA, M-FH, ST, FL, DH.

Investigation: JM-G, JWV-F, KS, MTK, RY, JA, LF, J-FJ, CB-W, AW, DC, EO, MP, CH, ML, IG, SA, M-FH, ST, FL, DH.
Visualization: JM-G, JWV-F, KS, MTK, RY, JA, LF, J-FJ, CB-W, AW, DC, EO, MP, CH, ML, IG, SA, M-FH, ST, FL, DH.
Funding acquisition: FL, CB-W, DH.
Project administration: FL, DH.
Supervision: FL, DH.
Writing – original draft: JM-G, JWV-F, FL, DH.
Writing – review & editing: JM-G, JWV-F, KS, MTK, RY, JA, LF, J-FJ, HY, CB-W, AW, DC, EO, MP, CH, ML, IG, SA, M-FH, ST, FL, DH.

Abstract

Rationale: During development, the contribution of IL34, a ligand of macrophage colony stimulating factor receptor (MCSFR), has not been fully defined. Together with its twin cytokine MCSF, they display an essential role in macrophage differentiation and activation, including tissue specialized macrophages. The mechanism of action of each molecule involves the phosphorylation of MCSFR in varying intensity and kinetics. Furthermore, IL34 can interact with other receptors and cofactors, opening a wide range of modulations during development. The aim of this work was to investigate these effects through the suppression of IL34 in different animal models and study molecular interactions, with a particular focus on osteoclast / osteoblast regulation.

Methods: Two different and unique models of *IL34*$^{-/-}$ were generated in zebrafish and mouse. The skeleton of both species was analyzed and compared by histological and morphometric (Micro-CT) approaches. The role of IL34 and new partners in osteoclast and osteoblast differentiation was analyzed by multiple techniques including mineralization assays, tartrate resistant acid phosphatase (TRAP) staining, receptor phosphorylation and activation assays, and gene expression (real-time quantitative PCR) studies. Furthermore, protein interactions were studied by surface plasmon resonance approach and protein-protein docking ClusPro analysis.

Results: Significant growth delay and hypo-mineralization of skeletal elements were observed in both *IL34*$^{-/-}$ models, as well as craniofacial dysmorphoses in mice. With regard to bone cells, an unexpected increase in the number of osteoclasts and an accumulation of pre-osteoblasts were observed in mice lacking IL34. For the first time, *in vitro* analyses complemented by protein binding and molecular docking studies established that IL34 interacts directly with certain Bone Morphogenetic Proteins (BMPs), modulating their various activities such as the stimulation of osteoblast differentiation.

Conclusions: A new mechanism of action for IL34 through BMPs has been characterized. IL34 interactions with MCSFR and BMPs appear crucial for both osteoclastogenesis and osteoblastogenesis, impacting bone tissue homeostasis and development. The potential interaction of IL34 with different members of the BMP family and their functional impact, including pathological situations such as cancer, should be further explored, opening new therapeutic perspectives.

Keywords: development, bone homeostasis, osteoclastogenesis, osteoblastogenesis, protein docking.

Graphical Abstract

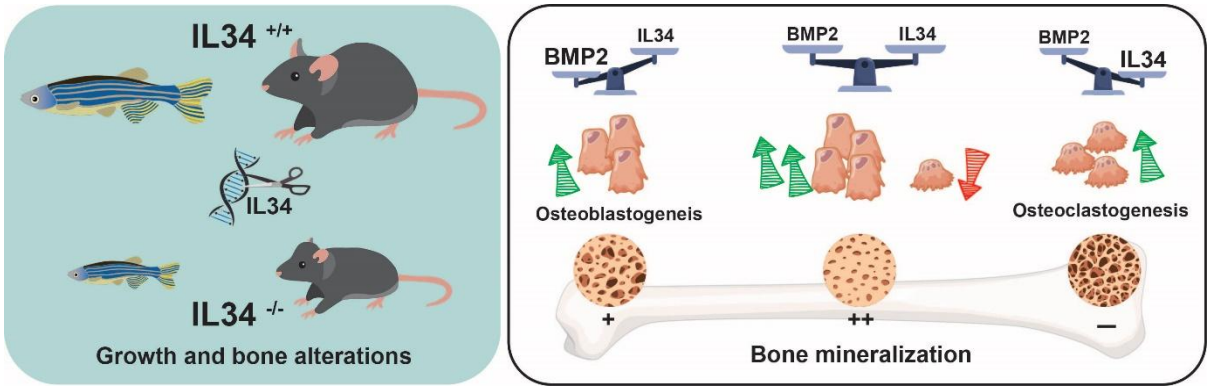

Introduction

Interleukin-34 (IL34) is a soluble cytokine discovered in 2008 by its ability to bind to macrophage colony-stimulating factor receptor (MCSFR), also known as c-FMS/CSF1R/CD115 [1]. This work has rekindled interest in the MCSFR signaling pathway and in the roles of the twin cytokines MCSF/IL34 in the differentiation and activation of myeloid cell lineage, such as macrophages, Langerhans cells, microglia cells and osteoclasts [2–5]. IL34 binding to MCSFR can occur as a homodimer or heterodimer with MCSF/CSF1, depending on the relative amounts of the two cytokines [6]. The twin cytokines induce similar patterns of phosphorylation of MCSFR but with variable intensity and kinetics, raising the question of their functional redundancy and specific functions. Their functional redundancy is confirmed by the greater severity of the bone phenotype associated with *MCSFR* versus *MCSF* invalidation in mice [7,8]. As far as the implications of IL34 during bone development are concerned, the data currently available are scarce, and focus mainly on its pro-osteoclastic action via its binding to the M-CSFR receptor (the binding that led to its identification [1]). Similarly to MCSF, IL34, by binding to MCSFR on the surface of osteoclastic precursors of myeloid origin, induces their engagement in the osteoclastic differentiation pathway which will then be completed by RANKL stimulation [2,9–14]. Regarding the source of IL34, osteoblastic expression [15,16] and chondroblastic expression [17] have been reported, suggesting that IL34 may be involved in communications between bone forming cells and osteoclasts. In the absence of a detailed description of the skeletal phenotype associated with IL34 invalidation during growth, the roles of IL34 in this growth process are still unclear. Additional receptors of IL34 have been identified and include Protein-Tyrosine Phosphatase β/ζ receptor (PTPβ/ζ) [18], Triggering Receptor Expressed on Myeloid cells-2 (TREM2) [19] and syndecan-1 [20]. PTPβ/ζ is mainly expressed by neuronal progenitors and glial cells and known as pleiotrophin/heparin-binding growth-associated molecule receptor [21]. TREM2 is a lipid-binding receptor [22], carried by myeloid lineage cells, whose differentiation and migratory capacities it modulates [23]. Finally, IL34 binds to Syndecan-1 (CD138) and this binding modulates IL34-mediated activation of MCSFR [20]. The diversity of IL34 receptors and co-ligands suggests that this cytokine plays an important role in the differentiation and activation of myeloid, neural and glial cells. In this context, the existence of other partners for IL34 must not be excluded. To analyze these functions, IL34 was suppressed in zebrafish and mouse and the phenotypes of these mutants was fully deciphered during development. New partners have been identified and their functional and biological implications have been analyzed.

Results

Zebrafish and mouse IL34 null models show significant alterations of the skeleton during development

IL34 invalidation was genetically achieved in zebrafish and mouse using respectively CrispR/Cas9 technology on one-cell stage embryos and conventional homologous recombination in embryonic stem cells.

Two zebrafish loss of function lines were generated for the single *Il34* allele, corresponding to a 23 bp deletion (mutant #1) and a 50 bp deletion with a 6 bp insertion (mutant 2) in exon 3 (**Figure 1A**; **Figure S1B-E**). In both zebrafish mutant lines, individuals at homozygous (-/-) status presented a severe growth alteration as shown in adult fish (**Figure 1B**). At 5 days post fertilization, both null mutations resulted in a poorer craniofacial skeletal mineralization (Von Kossa and alcian blue staining) comparatively to the control (+/+) but no evident dysmorphosis (**Figure 1C**, showed example for mutation #1).

The IL34 invalidated mouse line was obtained by CRE-recombinase activation on genetically modified *Il34* gene (**Figure 1D** and **Figure S2**) with LoxP sites in introns 2 and 5 enabling to remove exons 3 to 5 while maintaining a lacZ reporter sequence located in the 5' part of intron 2 ($Il34^{LacZ}$ allele in **Figure S2**). The functionality of the generated $Il34^{LacZ}$ allele was validated in the skin (**Figure S3**), a well-known site of IL34 expression (for instance [24,25]), with in mice homozygous for this allele (thereafter called $Il34^{-/-}$ mice), the expected absence of IL34 expression (**Figure S3A**) associated to a significant reduction of $CD207^{+}$ Langerhans cells (**Figures S3B-D**). The LacZ reporter was also functional as attested by the ß-galactosidase staining on skin section of mice heterozygous for the $Il34^{LacZ}$ allele (**Figure S3E**). $Il34^{-/-}$ mice were phenotypically altered. Indeed, 15 days-old IL34 invalidated mice exhibited a severe growth delay and dysmorphoses in whole skeleton elements, specifically in the craniofacial skeleton associated with hydrocephaly (**Figure 1E**). MicroCT scan 3D reconstructions of skull and tibia enabled visualization of these growth defects in $Il34^{-/-}$ mice (**Figure 1F,** red arrowheads). Morphometric analysis evidenced significant reduction in the skull growth in all planes (sagittal, vertical and transversal) and of the long bone growth in the length and width dimensions in $Il34^{-/-}$ mice compared to wild type (WT) (red vs black values in **Figure 1H** and **Figure S4A**). However, a significant augmentation was observed for the middle cranial vault and no impact was reported on the cranial vault length and the inter-zygomatic root width. Interestingly, the use of a murine IL34 blocking antibody (Sheff.5 clone) during the first post-natal week in WT mouse pups (protocol described in **Figure S4B**) similarly induced skull growth alterations in all planes but to a lower extent when compared to WT mice (brown vs black values in **Figure 1H**). MicroCT scans were also used to determine bone structure parameters and bone mineral density (BMD) in various anatomical sites, namely the mandibular, the vertebral, the cranial and the tibial bones. No significant difference in the trabecular thickness (Tb.Th), the trabecular space (Tr. Sp) or the percentage of bone volume (BV/TV) was observed between $Il34^{+/+}$ and $Il34^{-/-}$ mice whichever bone was considered (**Figure S4C** and **Figure 2C**, red vs black values). On the contrary, the trabecular number (Tb.N) was significantly increased only for the vertebral bone in $Il34^{-/-}$ (**Figure S4C**). Injections of the Sheff.5 blocking antibody had no impact on the bone structure parameters (**Figure S5**). Regarding the bone mineral density, a significant reduction in bone mineralization was observed in the cranial and the tibial bones of $Il34^{-/-}$ mice compared to $Il34^{+/+}$ mice (**Figures 2A-B and D**). The Sheff.5 antibody transitory treatment was insufficient to induce a similar bone mineral reduction in WT mice (**Figure 2A**, **Figure S5**).

Taken together, all those data demonstrated that IL34-invalidaton during development induces important bone modifications.

The absence of IL34 alters the osteoclast-osteoblast balance and bone homeostasis.

Histological analyses on tibia sections performed at the level of the proximal epiphysis (Safranin-O staining **Figure 2E**; Masson's trichrome staining **Figure S6**) revealed an important reduction in the growth plate hypertrophic chondrocytes area (*Il34*$^{+/+}$ 0.277 ± 0.021 mm^2 and *Il34*$^{-/-}$ 0.146 ± 0.094 mm^2). Tartrate resistant acid phosphatase (TRAP) and Osterix (Osx/SP7) dual staining carried out by histoenzymology and immunohistochemistry respectively (**Figure 2F** and top panel **Figure S7** for higher magnification) outlined an increase of both staining corresponding to osteoclastic (red stain) and pre-osteoblastic cells (brown stain) in the null mutant comparatively to the wild-type (*Il34*$^{+/+}$) littermate (**Figure 2F**). Interestingly, the RUNX2 immunohistochemistry staining, which enables identification of cells of the osteoblastic lineage (**Figure S8,** top panels), showed no difference in the number of stained cells between *Il34*$^{-/-}$ and *Il34*$^{+/+}$ mice, suggesting a slowdown of the osteoblast differentiation process with an accumulation of Osterix-positive pre-osteoblasts in the null mutant and without reduction of the total number of cells committed in this process.

To identify the part of the *Il34*$^{-/-}$ mouse skeleton phenotype linked to the increased number of osteoclastic cells, a RANKL blocking antibody (IK22.5) was injected during the first postnatal week to totally block the osteoclastogenesis (protocol described in **Figure S4B**). Such blockade had no consequence on the morphometric parameters in the null mutant (green vs red in **Figure 1G**) but impacted the trabecular parameters, the BV/TV and the BMD with significant differences for cranial and tibial bones (green vs red in **Figure S4C** and **Figures 2C-D**). Histological analyses on tibia sections performed at the level of the proximal epiphysis enabled visualization in the null mutant treated with the IK22.5 blocking antibody of a massive reduction of the TRAP positive cells (**Figure 2F** and bottom panels in **Figure S7**) associated with an apparent normalization of the growth plate hypertrophic chondrocytes area from 0.146 ± 0.094 mm^2 to 0.250 ± 0.033 mm^2 (**Figure 2E**) whereas no impact was noticed on the number of Osterix-positive (**Figure 2F** and **Figure S7**) and RUNX2-positive (**Figure S8**) cells.

Overall, these results suggested that IL34 may directly impact osteoblastic differentiation during development.

IL34 improves BMP2 activity in osteoblastic differentiation

BMPs and TGFβs proteins are direct involved in skeletal development and bone homeostasis (nicely reviewed in [26]). Interestingly, Interestingly, conditional knockout BMP2 and BMP4 mice described in the literature have a phenotype similar to our *Il34*$^{-/-}$ mouse model, with small body size and cranial and growth plate defects [27]. BMPs and TGFβs signaling pathways are crucial for proper osteoclast and osteoblast differentiation and maturation by regulating key transcriptional factors as NF-kβ in bone marrow monocytes and RUNX2 in mesenchymal stem cells. In order to see if those phenotypic and histological defects observed in *Il34*$^{-/-}$ models could be due to unknown interactions between IL34 and BMPs / TGFβs

members we performed *in vitro* studies to evaluate the impact of IL34 in BMPs / TGFβs signaling during osteoblastogenesis and osteoclastogenesis.

In vitro human mesenchymal stem cell differentiation into osteoblasts was induced by a standard osteoblastic differentiation medium (composition described in the Methods section). This differentiation, quantified by the phosphocalcic mineral deposition (alizarin red staining). and the expression levels of differentiation markers (*RUNX2*, *ALP* and *OCN*), was accelerated by addition of the bone morphogenic protein 2 (BMP2) at 10 ng/mL as shown in **Figure 3A-B**, **Figure S9** and **Figure S10**. The addition of IL34 alone (20 ng/mL) to the differentiation medium had no impact on the rate of osteoblastic differentiation, but interestingly it was able to potentiate the effect of BMP2 when added in combination with an optimal IL34/BMP2 concentration ratio (ng/mL) of two (**Figure 3A**). This concentration ratio corresponded to an equal amount in molarity of the two cytokines (**Figure S11A**). The combination of both molecules resulted in an earlier formation of calcium phosphate crystals (identifiable by alizarin red staining) (**Figure 3A** and **Figure S9**). No mineralization was observed in osteoblasts cultured in basic culture medium (CT-) neither in the presence alone or in combination of BMP2 and IL34 (data not shown). The expression levels of osteoblast differentiation markers were in agreement with the alizarin red staining. Indeed, the combination of both molecules impacted the expression of early (*RUNX2*) and late (*ALP* and *OCN*) markers of osteoblastogenesis in the way of a more rapid differentiation clearly visible from day 3 for *RUNX2* and at day 14 for *ALP* and *OCN* (**Figure 3B** and **Figure S10**). These data suggest a potentiation of BMP2 functions induced by IL34.

To validate this hypothesis, the canonical BMP signaling pathway was analyzed by Western blots in human mesenchymal stem cells. IL34 treatment resulted in an increased and earlier phosphorylation of the SMAD1/5 proteins observed in the presence of BMP2 compared to each molecule alone (Figure 3C). Due to the amount of human mesenchymal stem cells required for Western blot analysis, we decided to use an osteoblastic human osteosarcoma cell line (MNNG-HOS). This cell line recapitulated the same effect in SMAD1/5 phosphorylation of IL34 treatment in the presence of BMP2 **(Figure 4A**), BMP4 and BMP7 (**Figure S11B-E**), whereas IL34 has no similar impact on the phosphorylation of the SMAD2 protein induced by the TGFβ (**Figure 4A**, **Figure S12**). Interestingly, the potentiation effect of IL34 was blocked by the use of a specific human-IL34 blocking antibody named BT34 (**Figure 4B**, **Figure S12**), and the blocking of BMP2 pro-differentiation signaling with its natural inhibitor NOGGIN was annihilated by the presence of IL34 (**Figure 4C**, **Figure S12**). The potentiation effect of IL34 was moreover rapid (**Figure 4D**, **Figure S12**) and as previously mentioned sensitive to the ratio between the two cytokines (**Figure 4E-G, Figure S12**). The combination of BMP2 at 10 ng/mL to IL34 at 20 or 40 ng/mL induced higher SMAD1/5 phosphorylation than those observed with BMP2 alone, while the combination of BMP2 at 10 ng/mL and IL34 at 80 or 100 ng/mL significantly reduced SMAD1/5 phosphorylation (**Figure 4E**, **Figure S12**). The addition of IL34 at 20 ng/mL to BMP2 at 5, 10 or 20 ng/mL induced higher SMAD1/5 phosphorylation than those observed with BMP2 alone, while the combination of IL34 at 20 ng/mL and BMP2 at 40 or 80 ng/mL decreased SMAD1/5 phosphorylation (**Figure 4G**, **Figure S12**). This observation supported the

existence of a physical and strong functional interaction between IL34 and some proteins of the BMP family.

To complete the evidence on a physical interaction between IL34 and members of the BMP protein family, the potential impact of BMP2 addition on the IL34-induced osteoclastogenesis was evaluated *in vitro*. Differentiation of human $CD14^+$ cells into osteoclasts can be achieved by a two-step protocol corresponding to a 3-days culture period in the presence of MCSF (25 ng/mL) or IL34 (100 ng/mL) to the culture medium, followed by an 8-days period in presence of MCSF or IL34 combined to RANKL (100 ng/mL). Osteoclasts were identified in the culture by their expression of the TRAP activity (TRAP histoenzymology: purple staining). As previously shown [28], BMP2 addition to the cell cultures (concentrations from 1 to 50 ng/mL) may replace either MCSF or IL34 during the second period. However, while the combined addition of BMP2 (concentrations from 1 to 50 ng/mL) and MCSF to RANKL had no impact on the osteoclastogenesis, the combined addition of BMP2 and IL34 to RANKL induced a reduction of the number of osteoclasts formed (**Figure 3D-E**). Furthermore, the phosphorylation of MCSFR in response to IL34 was inhibited in presence of BMP2 and this inhibition was reversed by addition of NOGGIN supporting the existence of a functional physical link between IL34 and some members of the BMP protein family (**Figure 4H**, **Figure S12**).

Physical interactions between IL34 and some members of BMPs and receptors

To definitively establish the physical interaction between IL34 and BMPs, surface plasmon resonance experiments were performed and demonstrated effective binding of IL34 to BMP2, BMP4 and BMP7 with KD values of 3.63E-07 M, 4.26E-07 M and 9.22E-07 M respectively (**Figure 5A** and **Figure S13**).

A molecular modelling approach (see Materials and Methods), corresponding to a protein-protein docking study, established that IL34 binding to BMP2 occurred at the "Knuckle" sites of the BMP2 dimers known to correspond to the binding sites of BMP type 1 receptors and did not impinge on the "Wrist" sites that correspond to the binding sites of BMP type 2 receptors (**Figure 5B-D**; **Figure S14**). The amino acids of BMP2 and IL34 involved in binding were identified (**Figure 5E** and **Figure S15**), with BMP2 involving a pocket (formed by F305, W310, W313, Y385 and M388) in which the phenylalanine in position 85 for BMPR1A (F85) or the arginine in position 48 for IL34 (R48) are positioned during their respective interactions (Figure 5F). It is important to note that the amino acids involved are phylogenetically highly conserved in both BMP2 and IL34 and that, in addition, the amino acids of BMP2 implicated are also found conserved in several members of the BMP family (**Figure S16**). It was therefore possible to model the binding to IL34 of certain BMPs for which crystallographic structures were available, such as BMP3, BMP6 and BMP7 (**Figure S17**). The existence of direct physical links between BMP proteins and IL34 having been established, the question of the consequences of these links on the binding of BMPs to their receptors on the one hand and the binding of IL34 to MCSFR on the other was raised. Binding of BMP2 to the type 1 BMP receptor is hindered by IL34, which binds to the same

site as shown above. It should be noted that this "Knuckle" site is also the binding site for co-receptor proteins of the RGM family (**Figure S14C**) and that it is partially masked by NOGGIN binding (**Figure S14D**). With regard to the binding of BMP2 to type 2 BMP receptors, modelling shows that binding of the ACVR2A receptor, for example, is entirely possible on a BMP2 dimer with two IL34 binders (**Figure 6A**), the "Wrist" sites not being masked by the presence of IL34. These different possibilities for binding type 1 and 2 receptors and IL34 to a BMP2 dimer are shown in 3D in **Movie S1**. Concerning the binding of IL34 to MCSFR, the binding of IL34 to BMP2 occurs at a site that overlaps with the binding site of MCSFR to IL34 (**Figure 6B**), preventing the simultaneous binding of MCSFR and BMP2 to IL34.

Discussion

IL34, one of the latest cytokines identified [29], has been shown to bind to a variety of receptors with consequences for the differentiation and activation of myeloid, neural and glial cells (For review [4,5]). Surprisingly, the implications of this cytokine during development and growth had not been addressed in detail, unlike those of its receptor MCSFR (for review [30]), although its ability to stimulate differentiation of osteoclasts, cells important for skeletal growth, had been established via binding and activation of this receptor [13,14,31]. The primary aim of the work presented here was to determine these implications by generating two *in vivo* models of IL34 invalidation, one in zebrafish and the other in mice, and to characterize the associated skeletal phenotypes. Both models showed significant growth retardation, with reductions in cartilage mineralization in zebrafish and bone mineralization in mice. Concerning bone mineral density (BMD), the observation in *Il34*$^{-/-}$ mice of a significant reduction of this parameter only in certain bones raises questions. Interestingly, a dichotomy was observed between bones with endochondral mineralization (mandible, vertebrae, tibia trabecular zone (metaphyseal)) and those with intramembranous mineralization (cranial bone, tibia periosteal zone (diaphyseal)), the latter being the only ones to show a reduction in BMD. To decipher the molecular basis of such a difference, further studies will be required, focusing on the expression of all the factors involved in these two types of mineralization (matrix proteins, nucleation factors, enzymes, etc.).

In mice invalidated for IL34, obtained at an expected frequency (Mendelian inheritance) but with a reduced life expectancy (3 weeks), significant craniofacial dysmorphoses were observed with the presence of hydrocephalus. Such defects in craniofacial development are consistent with the previously established implications of IL34 in neural and microglial cells differentiation and activation [24,32–38]. This model should therefore provide a useful additional tool for deciphering the precise functions of IL34 during normal and pathological development of the central nervous system.

Histological study of bone tissue from *IL34*-invalidated mice revealed a marked increase in the number of osteoclasts in the growth plate, in contrast to the phenotype envisaged for the loss of a factor known to stimulate osteoclastogenesis [10,12,13]. As this increase in osteoclast numbers was associated with an accumulation of pre-osteoblasts (OSX-positive)

and a reduction in the hypertrophic zone of the growth plate, the question of a role for IL34 in the differentiation of osteoblasts and chondroblasts was raised. To check whether these two points were simply not secondary to the increase in osteoclastogenesis, the consequences of inhibiting RANKL (a factor essential to osteoclastogenesis) during the first week of life in *Il34*$^{-/-}$ mice were analyzed. No impact was observed on the accumulation of OSX-positive cells, while normalization of the size of the hypertrophic zone was observed. These results suggest that IL34 may directly regulate osteoblastic differentiation and probably indirectly that of chondroblasts via osteoclasts, bearing in mind that in inflammatory situations, both mature osteoblasts and hypertrophic chondrocytes can become important sources of pro-osteoclastic IL34 [16,39,40]. Interestingly, a relationship has already been observed between the level of osteoclastic activity and the size of the hypertrophic zone of the growth plate, and vice versa. Thus, a decrease in the hypertrophic zone goes hand in hand with an increase in osteoclastic activity [41,42] and an increase in this zone with a decrease in osteoclastic activity [43–47]. It should then be noted that the disruption of one or other of the elements in this relationship, over and above the repercussions on the other, induces growth retardation in all cases, as has been reported in patients with disorders of osteoclastogenesis (for example, in patients suffering from juvenile osteoporosis [48] or osteopetrosis [49]) as well as in those with chondrodysplasia (for review [50]). The increase in osteoclasts observed in *Il34*$^{-/-}$ mice, appropriately associated with a reduction in the hypertrophic zone of the growth plate, could therefore explain the growth retardation. Establishing the origin of the increase in osteoclasts in relation to the absence of IL34 was not immediately obvious. Osterix expression marks pre-osteoblasts, which are known as an important source of RANKL during growth [51,52]. The accumulation of OSX-positive cells at the subchondral level in *Il34*$^{-/-}$ mice could explain the increased number of osteoclasts, taking into account that an analysis of the number CD11b-positive cells (osteoclast precursors) in the bone marrow and spleen of *Il34*$^{-/-}$ mice reveled a marked increase (**Figure S18**). The question then arose as to the origin of the accumulation of these OSX-positive pre-osteoblasts in *Il34*$^{-/-}$ mice, given that the total number of cells committed to osteoblastic lineage according to RUNX2 labeling did not appear to be affected. An impact of IL34 absence on osteoblastogenesis was therefore strongly suspected.

Members of the TGFβ-BMP family, in particular BMP2, are major stimulators of osteoblastogenesis (for review [26]). The co-addition of IL34 with BMP2 in the culture medium of mesenchymal stem cells undergoing osteoblastic differentiation has shown, for certain ratios, a potentiation of the effect of BMP2 on this differentiation. Protein binding studies showed that IL34 could bind directly to BMP2, and 3D modeling identified the amino acids involved in this binding in the sequences of IL34 and BMP2. With regard to the BMP family, the amino acids involved in IL34 binding were found to be highly conserved, and the veracity of the direct binding of BMP4 and BMP7 to IL34 was established, suggesting that IL34 may potentiate the effects of several family members. IL34 binds to the "Knuckle" site of BMP2, which is also the binding site for type 1 receptors to BMPs, without obscuring the "Wrist" binding site for type 2 receptors. Protein binding studies have also shown that IL34 can directly bind type 2 receptors to BMPs (**Figure S19**), enabling it to occupy the "Knuckle"

site of a BMP and transform it into a "Wrist"-like site. A biphasic mechanism of action associated with IL34 binding to BMP dimers can then be proposed (**Figure 6C-D**), corresponding to the progressive modification of the ratio between type 1 and 2 BMP receptors. Thus, in the absence of IL34, basal activity is observed with a receptor ratio of 2/2. Then with an amount of IL34 equivalent to that of BMP2, maximum activity is observed corresponding to a receptor ratio of 1/3. Finally, with an excess of IL34, zero activity is observed with a receptor ratio of 0/4. Interestingly, several studies have reported that in an inflammatory context, BMP2 could inhibit IL34 expression [53–55], suggesting the possible existence of a feedback loop of IL34 potentiation of BMP2 activity. The ratio of IL34 to BMP2 has also been shown to impact IL34 binding to the MCSFR so the osteoclastogenesis in bone. IL34 thus appears to play a key role in bone formation, modulating both osteoclastogenesis via its direct binding to the MCSFR and osteoblastogenesis via its binding to BMPs.

In a more general context, IL34's ability to directly control MCSF receptor activation and indirectly BMP receptors activation defines it as a major player in the development, growth, homeostasis and function of most organs. Further studies will obviously be needed to determine which members of the BMP family are IL34 partners in each organ, in normal physiology and pathological situations (for review [56]) including cancers for which IL34 is already presented as a therapeutic target of major interest [57–59].

Materials and Methods

In vivo experiments

All zebrafish (*Danio rerio*) used for this project were located in the aquaria at the Bateson Centre, at the University of Sheffield (UK). Zebrafish were present in tanks at a density of no more than four zebrafish per liter, with 14 hours light and 10 hours dark cycle, at a temperature of 28 °C. All experimental procedures were carried out in accordance with the UK Home Office Project License PPL70/8178 and personal license IO6008638. All transgenic mice (*Mus Musculus*) used for this project were housed under pathogen-free conditions at the Experimental Therapy Unit at the Faculty of Medicine of the University of Nantes, France (Agreement D44015 and DUO 6781). All protocols applied in the present study were first validated by the French ethical committee of the “Pays de la Loire” (CEEA-PdL-06) and authorized by the French ministry of agriculture and fisheries (authorization # 18415-201901101823350 v2).

Generation of IL34 mutant zebrafish

The zebrafish *Il34* gene (ENSDARG00000091003.2 or ZDB-GENE-050419-150) contains seven exons as human and mouse genes (**Figure 1**). IL34 mutant zebrafish was generated using the CRISPR-Cas9 technology as previously described [60,61]. Exon 3 was targeted using the sequence shown in **Figure S1A** and the corresponding 20 bp spacer region was placed into a guide RNA template for in *vitro* transcription. The gRNA was then transcribed using the MEGAshortscript T7 kit (Life Technologies, UK) and microinjected with Cas9

protein (NEB, UK) into the yolk of zebrafish embryos the one cell stage. F0 adult fish were crossed with wild-type fish to identify founder with germline transmission. Primers used for genotyping were (Fw 5'-TCA GCC AAT AAA TAT CAG ATC CA-3' and Rv 5'-CGT CTC CTG GTT GCA TTT-3') which amplify a 300 bp fragment of the WT sequence of zebrafish IL34 exon3 covering the chosen CRISPR target sequence. Obtained fragments of shorter sizes were sequenced to identify mutations induced in the different founders. Two mutations corresponding to a 23 bp deletion (mutant #1 in **Figure 1**) and a 50 bp deletion combined to a 6bp insertion (mutant #2 in **Figure 1**) were obtained. Phenotypes of zebrafishes homozygous for each of these mutations (*Il34*$^{-/-}$ from F3 or following generations) were compared to ensure for link to *Il34* deficiency and not from potential background mutations. Genotyping was performed on DNA extracted from the caudal fins by PCR using same primers as those used to identify founders. Fragments of 300 bp, 277 bp and 256 bp were amplified respectively for *Il34* exon 3 WT, mutant #1 and mutant #2 sequences. Animal were studied at 5 days post fertilization or at 3 months after birth.

Van Kossa and Acian Blue staining of zebrafish skeleton

For Von Kossa staining, samples were fixed in 4% PFA for 2 h at room temperature, rinsed in water containing 0.01% tween 20, and left to incubate in a solution of silver nitrate under a 60 W light bulb for 1 h. After rinsing with water containing 0.01% tween 20, samples were fixed in 2.5% sodium-thiosulfate for 10 min, rinsed and again fixed in 4% PFA for 30 min at room temperature. Preservation was done in glycerol, and samples were kept at room temperature in dark until images were taken.

For Alcian Blue Staining, samples were fixed overnight in 4% PFA at 4 ºC. After several washes in a phosphate buffer solution containing 0.1% tween 20 (PBS-T) and dehydration using methanol, samples were transferred into Alcian blue staining solution (0.1% Alcian Blue, 70% ethanol, 1% concentrated hydrochloric acid) and left to stain overnight at room temperature. Samples where then rinsed in PBS-T and bleached in 30% hydrogen peroxide for 10 min at 37 ºC. A 30% saturated borate solution was then used to eliminate all residues of bleaching solution before putting the samples into a trypsin digestion solution for 30 min at 37 ºC until brains and eyes appeared translucent. A rehydration was performed, and samples were put in glycerol for preservation until images were taken.

Zebrafish were imaged for both stains using the SMZ1500 stereomicroscope, with a DS-Fi1 camera (both Nikon, Japan), at 20 X magnification and Nikon Elements software.

Generation of *Il34* mutant mouse

The *Il34* mutant mouse was generated at the Mouse Clinical Institute (IGBMC, Illkirch, France; Project IR00004258 / K4258) by classical embryonic stem cells (ES) injection in blastocyst stage embryo. Three JM8.N4 ES cell clones carrying the targeted Il34$^{tm1a(EUCOMM)Wtsi}$ allele were purchased at the European Conditional Mouse Mutagenesis Consortium (EUCOMM) and the clone EPD0146_4_F02 (embryonic stem line JM8.N4; C57BL/6) that was confirmed by PCR and Sanger sequencing (**Figure S2**) as being correctly targeted was used to generate the *Il34* conditional mutant mouse line. Breeding with ERT2-Cre mice (B6.Cg- Tg(UBC- cre/ERT2)1Ejb/J, JR#8085, Jackson Laboratory, Bar Harbor, Maine, USA) enabled to (Tamoxifen dependently) delete exons 3–5 of *Il34* and the

neomycin-resistance cassette generating the Il34$^{+/LacZ}$ mice (**Figure S2**). Breeding with CAG-FLPe mice (C57BL/6-Tg(CAG-flpe)16Ito, RBRC10707, RIKEN BRC, Tsukuba, Ibaraki 305-0074, Japan) allowed to delete the whole LacZ–NeoR cassette and generate mice carrying a loxP-flanked *Il34* allele (*Il34*$^{+/f}$). Homozygous *Il34*$^{LacZ/LacZ}$ mice (called *Il34*$^{-/-}$ in the manuscript) were used for analysis. Mice were genotyped by PCR (**Figure S2**) with the primers Il34-S2: 5'-GTC AGT ATC GGC GGA ATT-3', Il34-S3: 5'-GTT TGG CCG ATG CTG GCA AAG G-3' and Il34-AS2: 5'-CTG TCT TAT GAA GAT GGC ATG CC-3'. Il34-S2 and Il34-AS2 primers enable to amplify a 440 bp fragment in presence of *Il34*^{LacZ} allele, and Il34-S3 and Il34-AS2 primers fragments of 240 bp and 290 bp respectively in presence of wild type (WT) and *Il34*^{f} alleles (**Figure S2**).

Alizarin Red and Alcian Blue double staining of mouse skeleton

The whole-mount skeletal staining protocol used is derived from the protocol of Rigueur and Lyons [62]. Briefly, after euthanasia, all skin, internal organs, adipose tissue and as much as possible muscle were removed before fixation in a PBS 1X pH 7.4 solution containing 2% of paraformaldehyde and 0.2% glutaraldehyde. Skeletons were then dehydrated in ethanol and placed in acetone for permeabilization. Cartilage staining was then realized by submerging the skeletons in the Alcian blue stain (Alcian blue 8GX 0.03% (w/v), 80% EtOH, 20% glacial acetic acid). After washes in 70% and 95% ethanol, a pre-clear of the tissue was realized in a 1% KOH solution. Bone staining was then carried out in Alizarin red stain (Alizarin red 0.005% (w/v) in 1% (w/v) KOH). The Alizarin red solution was then replaced with a v/v mix of glycerol and 1% KOH to remove the excess red color. Skeleton were transferred to 100% glycerol for long-term storage and imaging.

New-born mice treatment with blocking antibodies

The protocol used to treat newborn mice with blocking antibodies was previously described [46]. Briefly, newborn C57BL/6 mice from naïve and transgenic *IL34*$^{+/LacZ}$ mothers received four subcutaneous injections (25 mg/kg of body weight) of respectively Sheff-5 (rat anti-mouse IL34 blocking IgG1 antibody, Diaclone, Besançon, France) and IK22-5 rat anti-mouse RANKL blocking IgG2a antibody [63] or isotopic corresponding control every 2 days beginning at day 1 after birth (**Figure S4B**). The mice were finally sacrificed at postnatal day 15 for phenotyping.

Micro-CT analysis

A Skyscan 1076 micro-CT scanner (Skyscan, Kontich, Belgium) was used to analyze and compare between the different groups of mice (at 15 days postnatal and n=8 for each group except for *Il34*$^{-/-}$ + IK22, n=4) the bone morphometric, structural and mineral parameters at different anatomical sites namely the tibia, the mandible, the vertebra and the cranium. All samples were scanned using the same parameters (pixel size 9 μm, 50 kV, 0.5 mm Aluminum filter, 20 min of scanning). The scanner reconstruction was carried out using the NRecon software and the analyses were performed using CTAn, CTVox, and DataViewer software (Skyscan). In order to obtain the different measurements, the IMAGE-J software (National Institutes of Health, Bethesda, MD, USA) was used. In this way, the acquisition of the image

in CTVox was systematically calibrated with a phantom of 5 mm (known size) and all measurements were finally sized using the analysis scale in the IMAGE-J software.

Bone morphometric parameters including tibia total length and width were sized using specific reference marks (**Figure 1C** and **Figure S4A**), and for the cranium measurements were made using the method previously described [64]. Briefly, seven measurements regarding the sagittal, vertical and transversal planes of craniofacial growth were made (**Figure 1C** and **Figure S4A**).

Bone mineral and structural parameters including the bone mineral density (BMD), the percentage of bone volume (BV/TV), the trabecula thickness (Tb.Th), the trabecula separation (Tb.Sp) and the trabecula number (Tb.N) were analyzed for each bone at different anatomical sites using a volume of interest (VOI) measuring 2.0 mm x 1.1 mm × 1.1 mm. The VOI was sectioned using the Data Viewer software and analyzed using the CTAn software. The different points chosen for the analysis are presented in **Figure S4**. To facilitate the identification of changes in the different structures, a "color density range" was used in the CTAn software that made it possible to adjust the correspondence of color and brightness values using image gray scales. For tibia and head images, a brightness level of -32 and a contrast level of 6 from the color density range of the CTAn software were systematically used.

Histology, histoenzymology and immunohistochemistry

Histology, histoenzymology and immunohistochemistry were performed on 3 µm thickness paraffin embedded sections of the different samples prepared as previously described [65]. Masson's trichrome and Safranin-O stains were performed following classical protocols and tartrate-resistant acid phosphatase (TRAP) histoenzymology was carried out as previously described [66]. Immunohistochemistry was performed by using the protocol as previously described [67] and the following antibodies: rabbit monoclonal anti-RUNX2 (Abcam, ref#ab192256, 1/1000), rabbit polyclonal anti- osterix (OSX) (Abcam ref#ab22552, 1/1000), anti-CD207 (eBioscience, ref# 14-2073-80, 1/100).

LacZ staining

Sections (12µm) of *IL34*$^{+/LacZ}$ mice epidermis embedded in OCT were cut using Cryostat Leica CM3050S. Slices were fixed with PFA 1% 5 min, rinsed with PBS 1x and incubated in Xgal (5-bromo-4-chloro-3-indolyl-beta-D-galactopyranoside) solution overnight at 37 °C. Sections were rinsed with PBS 1X, left to dry and mounted with EUKITT® medium.

***In vitro* experiments**

Reagents

Recombinant human Macrophage-Colony Stimulating Factor (MCSF), human interleukin-34 (IL34), human M-CSF receptor (MCSFR/CD115), human TGF-β1, human bone morphogenetic protein 2 (BMP2), human bone morphogenetic protein 4 (BMP4), human bone morphogenetic protein 7 (BMP7), human Noggin, Activin RIIA receptor (ActRIIA), human Activin RIIB receptor (ActRIIB), human TRANCE (RANKL) and antibody anti-human M-CSFR, Anti-Phosho-M-CSFR (Y723) were obtained from R&D Systems (Abingdon, UK). Anti-human IL34 (BT-34) mouse IgG1 monoclonal antibody was produced

by Diaclone (Besançon, France) under patent (Heymann D, Ségaliny A, Brion R. University of Nantes /Nantes Hospital/INSERM, "Anti-IL-34 antibodies". WO/2016/097420 A1, 2016). Antibodies directed against human Smad1 (D59D7), human Smad2 (D43B4), anti Phospho-Smad1/5 (ser463/465) (41D10), anti-phospho-Smad2 (Ser465/467) (138D), β-Actin (8H10D10) and HRP-conjugated secondary antibodies were purchased from Cell Signalling (Ozyme, Saint Quentin Yvelines, France). AlphaLISA® SureFire® Ultra Total SMAD1 and p-SMAD1 (Ser463/465) Assay kits were purchase from PerkinElmer (Villebon-sur-Yvette, France).

Cell cultures

The cell lines used in the present study were purchased from the American Tissue Cell Collection (ATCC, Molsheim, France). HEK293 (HEK) transfected with the pCDNA3 empty plasmid or the pCDNA3 plasmid containing the MCSFR gene as described by Segaliny et al., [6]. Human Mesenchymal Stem Cells-Bone Marrow (HMSC-BM) (CLS catalog number 300665, Lot.071222P2) and human MNNG/HOS osteosarcoma cell line (ATCC, catalog number CRL-1547) were cultured in Dulbecco's Modified Eagle's Medium (DMEM, Lonza, Levallois-Perret, France) supplemented with 10% fetal bovine serum (FBS; Hyclone Perbio, Bezons, France) and 2 mmol/L of L-glutamine. All the experiments using HMSC-BM cells were done at passage 2. For the Human MNNG/HOS osteosarcoma cell line experiments were performed between passage 2 and 4. All cell lines were regularly tested for the absence of mycoplasma.

Human osteoclast differentiation

$CD14^+$ monocytes were isolated from peripheral blood of 3 healthy donors $CD14^+$ cells were initially isolated from human peripheral blood donors provided by the French blood bank institute (Etablissement Français du Sang, Nantes, France, authorization number: NTS 2000-24), by using MACS microbeads (MiltenyiBiotec, Bergisch Gladbach, Germany) as previously described [68]. For osteoclast differentiation, $CD14^+$ cells were cultured in alpha-MEM (Lonza) supplemented with 10% human serum (Invitrogen, France) and in the presence of human MCSF (25 ng/mL) or human IL34 (100 ng/mL) +/- human BMP2 (40 or 100 ng/mL) for 3 days. Then cells were treated with same molecules in the presence of human RANKL (100 ng/mL) for 11 days. Medium was renewed every 3 days. After 11 days of treatment, osteoclasts were analyzed by Acid Phosphatase (TRAP) staining kits (Sigma Aldrich, Saint-Quentin Fallavier, France). $TRAP^+$ multinucleated cells with 3 nuclei and more were considered as osteoclasts and were manually enumerated.

Human osteoblastic differentiation

Human Mesenchymal Stem Cells-Bone Marrow (HMSC-BM) (CLS catalog number 300665) were purchased from CLS (Germany). Osteoblast differentiation assays were performed as previously described [67,69]. Briefly, HMSC-BM were cultured in DMEM was supplemented 10% of FBS, vitamin D3 (10^{-8} M; Sigma) and dexamethasone (10^{-7} M; Sigma). After 3 days, ascorbic acid (50 ng/mL; Sigma) and β-glycerophosphate (10 mM; Sigma) were added to allow mineralization detected by alizarin red-S staining for three weeks. Images were captured using a stereomicroscope (Nikon), and mineralized surfaces

were quantified using Image J software. Mineralization process was carried out in the presence or absence of human cytokine IL34 (25 ng/mL), BMP2 (10 ng/mL) or combination of both molecules for 3 weeks. RNA samples were collected at days 3, 4, 14 and 21 after the induction of differentiation.

Flow cytometry

FACS analysis of CD11b monocytic bone marrow and spleen cells were performed as previously described [70]. Briefly, after red blood cell lysis (Sigma-Aldrich), bone marrow and spleen cells were labelled with anti-CD11b (clone M1/70; BD Bioscience, Le Pont de Claix, France). Data were acquired using a FACS Canto-II (BD Biosciences).

Western blot

The cells were collected in a RIPA buffer (10 mM Tris pH 8, 1 mM EDTA, 150 mM NaCl, 1% NP40, 0.1% SDS containing a cocktail of protease and phosphatase inhibitors Halt™ (Thermo Fisher, Waltham, MA, USA). The protein concentration was determined using a BCA (bicinchoninic acid) method by BC Assay Protein Quantitation Kit (Interchim, Montluçon, France). 50 µg of protein extracts were prepared in a Laëmmli buffer (62.5 mM Tris–HCl, pH 6.8, 2% SDS, 10% glycerol, 5% 2-mercaptoethanol, 0.001% bromophenol blue) and then separated by SDS-polyacrylamide gel electrophoresis. After electrophoretic transfer, the immobilon-P membranes (Millipore, Molsheim, France) were blotted with the antibodies referenced in the "Reagents" section. The membranes were then probed with secondary antibodies coupled with horseradish peroxidase. Antibody binding was visualized with an enhanced chemiluminescence (ECL) kit Clarity™ Western ECL Substrate (Bio-Rad, Marnes-la-Coquette, France). The luminescence was detected with a ChemiDoc MP Imaging System (Bio-Rad). Blots images and semi-quantitative analysis were done using ImageJ software (USA). Each experiment was repeated at least 3 times.

SMAD1/5 signaling measured by Alpha SureFire® Technology

Direct quantification analysis of cell signaling was performed by using Alpha SureFire® Technology from PerkinElmer in a Victor® Nivo™ multimode microplate reader (ALSU-PSM1; PerkinElmer, Villebon-sur-Yvette, France).

RNA isolation and real-time PCR

Total RNA was extracted using NucleoSpin® RNA Plus (Macherey-Nagel, Duren, Germany). 1 µg of total RNA was used for first strand cDNA synthesis using the OneScript® RT Mix (Ozyme). Real-time PCR was performed on 20 ng of reverse transcribed total RNA (cDNA), 300 nM of primers (QuantiTect Primer® Assays, Qiagen) and PowerUp™ SYBR™ Master Mix from Applied Biosystems™ (Thermo Fisher) in a CFX96 Touch Deep Well Real-Time PCR Detection system from Bio-Rad. Thermal cycle conditions were perform by following manufacture protocol. The analysis was performed with CFX Manager Software (Bio-Rad) using human glyceraldehyde 3-phosphate dehydrogenase (GAPDH), Hypoxanthine Phosphoribosyl transferase 1 (HPRT1) and TATA box binding protein (TBP) as invariant controls (QuantiTect Primer® Assays, Qiagen). Oligonucleotides were designed with Primer-Blast software (NCBI) and purchased from Eurogentec (Eurogentec, Angers,

France). The $2^{-\Delta\Delta Ct}$ (cycle threshold) method was used to calculate expression levels. List of primers and gene name symbols with corresponding full names are indicated in Tables S1 and S2 below.

Table S1 Qiagen q-PCR murine primers

Official full name; Alias	**Official symbol**	**Gene Globe Id**
Alkaline phosphatase, liver/bone/kidney	ALPL	QT00012957
Osteocalcin or bone gamma-carboxyglutamate protein	BGLAP	QT00232771
Runt-related transcription factor 2; *CBFA1*	RUNX2	QT00020517
Tumor necrosis factor receptor superfamily, member 11b	TNFRSF11B	QT00014294
Macrophage Colony Stimulating Factor	MCSF	QT00035224
Macrophage Colony Stimulating Factor Receptor	MCSFR	QT00073276
Bone Morphogenetic Protein Receptor 1A	BMPR1A	QT00085358
Bone Morphogenetic Protein Receptor 2	BMPR2	QT00226065
Activin Receptor 2A	ACVR2A	QT00077749

Table S2: Eurogentec q-PCR murine primers

Official full name; Alias	**Official symbol**	**Gene Globe Id**
Interleukin-34	IL-34	Fwd 5'-GGA CAC ACT TCT GGG GAC A-3' Rev 5'-CCA AAG CCA CGT CAA GTA GG-3'
Langerin	CD207	Fwd 5'-TCA CCT CCA TTG TGC TTC AG-3' Rev 5'-ATC GTC CAC ACG ACC TCT TT-3'
Glyceraldehyde-3-phosphate dehydrogenase	GAPDH	Fwd 5'-TGC GAC TTC AAC AGC AAC TC-3' Rev 5'-CTT GCT CAG TGT CCT TGC TG-3'

Surface plasmon resonance (SPR) assays

All SPR experiments were performed on a T200 apparatus (Cytiva) at 25 °C in PBS pH 7.4 containing 0.05% of surfactant P20. Human recombinant BMP2, BMP4 and BMP7 proteins were immobilized (1500- 2300 RU) at pH 4.5 on CM5-S sensor chip by amine coupling following the manufacturer's instructions (Cytiva, Velizy-Villacoublay, France). IL34 kinetics were measured using one cycle titration, for these five increasing concentrations of recombinant human IL34 (12.5, 25, 50, 100, 200 nM) were injected during 60 s at 100 µL/min on coated BMPs. The last injection was followed by a 600 s dissociation time in running buffer. The KD values were evaluated using a bivalent fitting model (T200 Evaluation software 3.2.1, Cytiva). All sensorgrams were corrected by subtracting the low signal from the control reference surface (without any immobilized protein) and blank buffer injections before fitting. For KD evaluation of IL34 on human recombinant receptors

BMPRIIA, Act RIIA and Act RIIB, these receptors were captured on immobilized anti-human Fc (Cytiva), four increasing concentrations of IL34 (18.75, 37.5, 75, 150, 300 nM) were injected. The KD values were evaluated by using a steady-state fitting model. The binding responses of IL34 (50 nM) alone, Nogging (50 nM) alone and a mixing of IL34 and Noggin were measured by 180 s injection on different coated BMP proteins (BMP2, BMP4, BMP7) at a flow rate of 30 µL/min followed by a dissociation time of 400 s in running buffer.

Protein-Protein docking and analysis

Structures of M-CSFR, BMPR1 and IL-34 were extracted from their bound crystallographic forms (1REW for BMPR1A + BMP2 [71], 4WRL for M-CSF:M-CSFR1 [72] and 4DKD for IL-34:M-CSFR1 [73]). Docking experiments were performed using either BMP-2 fixed and the partner protein mobile, or the reverse, as previously published [71]. ClusPro analysis [74] was performed in balanced mode, only the first 10 binding modes clusters were considered for analysis, the best modes were selected by visual inspection. Interface analysis was performed using the PISA web server [75]. Visualization and superimposition of docking poses and crystallographic structures were done using PyMOL (The PyMOL Molecular Graphics System, Version 2.5 Schrödinger, LLC; Schrödinger, LLC 2015).

Statistical analysis

All experiments were repeated at least three times in independent experiments. The differences between the experimental conditions were assessed with Student's t test or a one-way ANOVA followed by the Mann–Whitney test or Kruskal-Wallis test (in the case of more than two independent samples of equal or different sample size). The results are given as a mean ± SD. Results were considered significant at p-values of ≤ 0.05, p-values of ≤ 0.01 and p-values of ≤ 0.001. GraphPad Prism 6 software (GraphPad Software, San Diego, CA, USA) and Real Statistics Resource Pack Software (Release 8.91), copyright (2013-2023) Charles Zaiontz (www.real-statistics.com) were used for statistical analyses.

Supplementary Material

Supplementary information is available in Supplementary File.

Acknowledgments

The authors wish to thank members from the Therapeutic Experimental Unit (Nantes, France) for their technical assistance.

Funding

Il-34$^{-/-}$ mice were generated at the "Institut Clinique de la Souris" (Illkirch-Graffenstaden, France) and their development was supported by an INSERM grant (Project IR00004258 / K4258). The work was supported by a maturation grant funding program of the Ouest Valorisation Technology Transfer Office (SATT Ouest Valorisation, Nantes, France; ref. DV2439) and by Agence Nationale de la Recherche (ANR-20-CE14-0037).

Data sharing

The authors of this investigation declare that all the data, analytical methods, and study materials are available to the researchers. All the details information is available in Supplemental Data.

Conflict of interests

Authors declare that they have no competing interests.

References

1. Lin H, Lee E, Hestir K, et al. Discovery of a cytokine and its receptor by functional screening of the extracellular proteome. Science. 2008; 320: 807–11.

2. Nakamichi Y, Udagawa N, Takahashi N. IL-34 and CSF-1: similarities and differences. J Bone Miner Metab. 2013; 31: 486–95.

3. Stanley ER, Chitu V. CSF-1 receptor signaling in myeloid cells. Cold Spring Harb Perspect Biol. 2014; 6: a021857.

4. Baghdadi M, Umeyama Y, Hama N, et al. Interleukin-34, a comprehensive review. J Leukoc Biol. 2018; 104: 931–51.

5. Muñoz-Garcia J, Cochonneau D, Télétchéa S, et al. The twin cytokines interleukin-34 and CSF-1: masterful conductors of macrophage homeostasis. Theranostics. 2021; 11: 1568–93.

6. Ségaliny AI, Brion R, Brulin B, et al. IL-34 and M-CSF form a novel heteromeric cytokine and regulate the M-CSF receptor activation and localization. Cytokine. 2015; 76: 170–81.

7. Dai X-M, Ryan GR, Hapel AJ, et al. Targeted disruption of the mouse colony-stimulating factor 1 receptor gene results in osteopetrosis, mononuclear phagocyte deficiency, increased primitive progenitor cell frequencies, and reproductive defects. Blood. 2002; 99: 111–20.

8. Dai X-M, Zong X-H, Akhter MP, Stanley ER. Osteoclast Deficiency Results in Disorganized Matrix, Reduced Mineralization, and Abnormal Osteoblast Behavior in Developing Bone. Journal of Bone and Mineral Research. 2004; 19: 1441–51.

9. Tarabeih N, Shalata A, Kalinkovich A, Higla O, Livshits G. Elevated circulating levels of IL-34 are strongly associated with osteoporosis. Arch Osteoporos. 2023; 18: 132.

10. Amarasekara DS, Yun H, Kim S, Lee N, Kim H, Rho J. Regulation of Osteoclast Differentiation by Cytokine Networks. Immune Netw. 2018; 18: e8.

11. Cheng X, Wan Q, Li Z. AG490 suppresses interleukin- 34- mediated osteoclastogenesis in mice bone marrow macrophages. Cell Biology International. 2017; 41: 659–68.

12. Nakamichi Y, Mizoguchi T, Arai A, et al. Spleen serves as a reservoir of osteoclast precursors through vitamin D-induced IL-34 expression in osteopetrotic op/op mice. Proc Natl Acad Sci U S A. 2012; 109: 10006–11.

13. Chen Z, Buki K, Vääräniemi J, Gu G, Väänänen HK. The critical role of IL-34 in osteoclastogenesis. PLoS One. 2011; 6: e18689.

14. Baud'huin M, Renault R, Charrier C, et al. Interleukin-34 is expressed by giant cell tumours of bone and plays a key role in RANKL-induced osteoclastogenesis. J Pathol. 2010; 221: 77–86.

15. Yu Y, Yang D, Qiu L, Okamura H, Guo J, Haneji T. Tumor necrosis factor-α induces interleukin-34 expression through nuclear factor-κB activation in MC3T3-E1 osteoblastic cells. Molecular Medicine Reports. 2014; 10: 1371–6.

16. Eda H, Shimada H, Beidler DR, Monahan JB. Proinflammatory cytokines, IL-1β and TNF-α, induce expression of interleukin-34 mRNA via JNK- and p44/42 MAPK-NF-κB pathway but not p38 pathway in osteoblasts. Rheumatol Int. 2011; 31: 1525–30.

17. van Eegher S, Perez-Lozano M-L, Toillon I, et al. The differentiation of prehypertrophic into hypertrophic chondrocytes drives an OA-remodeling program and IL-34 expression. Osteoarthritis Cartilage. 2021; 29: 257–68.

18. Nandi S, Cioce M, Yeung Y-G, et al. Receptor-type protein-tyrosine phosphatase ζ is a functional receptor for interleukin-34. J Biol Chem. 2013; 288: 21972–86.

19. Xie X, Zhang W, Xiao M, et al. TREM2 acts as a receptor for IL-34 to suppress acute myeloid leukemia in mice. Blood. 2023; 141: 3184–98.

20. Segaliny AI, Brion R, Mortier E, et al. Syndecan-1 regulates the biological activities of interleukin-34. Biochim Biophys Acta. 2015; 1853: 1010–21.

21. Maeda N, Noda M. Involvement of receptor-like protein tyrosine phosphatase zeta/RPTPbeta and its ligand pleiotrophin/heparin-binding growth-associated molecule (HB-GAM) in neuronal migration. J Cell Biol. 1998; 142: 203–16.

22. Colonna M. The biology of TREM receptors. Nat Rev Immunol. 2023; 23: 580–94.

23. Shang J, Xu Y, Pu S, Sun X, Gao X. Role of IL-34 and its receptors in inflammatory diseases. Cytokine. 2023; 171: 156348.

24. Greter M, Lelios I, Pelczar P, et al. Stroma-derived interleukin-34 controls the development and maintenance of langerhans cells and the maintenance of microglia. Immunity. 2012; 37: 1050–60.

25. Croquette M, Faugeroux A, Fonlupt C, et al. IL-34 Exerts Anti-Inflammatory Activities on Keratinocytes and Is Downregulated in Psoriatic-Inflamed Skin. J Invest Dermatol. 2023; 143: 2521-2524.e5.

26. Wu M, Wu S, Chen W, Li Y-P. The roles and regulatory mechanisms of TGF-β and BMP signaling in bone and cartilage development, homeostasis and disease. Cell Res. 2024; 34: 101–23.

27. Shu B, Zhang M, Xie R, et al. BMP2, but not BMP4, is crucial for chondrocyte proliferation and maturation during endochondral bone development. Journal of Cell Science. 2011; 124: 3428–40.

28. Jensen ED, Pham L, Billington CJ, et al. Bone morphogenic protein 2 directly enhances differentiation of murine osteoclast precursors. J Cell Biochem. 2010; 109: 672–82.

29. Catalan-Dibene J, McIntyre LL, Zlotnik A. Interleukin 30 to Interleukin 40. J Interferon Cytokine Res. 2018; 38: 423–39.

30. Chitu V, Stanley ER. Regulation of Embryonic and Postnatal Development by the CSF-1 Receptor. Curr Top Dev Biol. 2017; 123: 229–75.

31. Boström EA, Lundberg P. The newly discovered cytokine IL-34 is expressed in gingival fibroblasts, shows enhanced expression by pro-inflammatory cytokines, and stimulates osteoclast differentiation. PLoS One. 2013; 8: e81665.

32. Nandi S, Gokhan S, Dai X-M, et al. The CSF-1 receptor ligands IL-34 and CSF-1 exhibit distinct developmental brain expression patterns and regulate neural progenitor cell maintenance and maturation. Dev Biol. 2012; 367: 100–13.

33. Wang Y, Szretter KJ, Vermi W, et al. IL-34 is a tissue-restricted ligand of CSF1R required for the development of Langerhans cells and microglia. Nat Immunol. 2012; 13: 753–60.

34. Ma D, Doi Y, Jin S, et al. TGF-β induced by interleukin-34-stimulated microglia regulates microglial proliferation and attenuates oligomeric amyloid β neurotoxicity. Neurosci Lett. 2012; 529: 86–91.

35. Wang Y, Colonna M. Interkeukin-34, a cytokine crucial for the differentiation and maintenance of tissue resident macrophages and Langerhans cells. Eur J Immunol. 2014; 44: 1575–81.

36. Chitu V, Gokhan Ş, Nandi S, Mehler MF, Stanley ER. Emerging Roles for CSF-1 Receptor and its Ligands in the Nervous System. Trends Neurosci. 2016; 39: 378–93.

37. Wu S, Xue R, Hassan S, et al. Il34-Csf1r Pathway Regulates the Migration and Colonization of Microglial Precursors. Dev Cell. 2018; 46: 552-563.e4.

38. Easley-Neal C, Foreman O, Sharma N, Zarrin AA, Weimer RM. CSF1R Ligands IL-34 and CSF1 Are Differentially Required for Microglia Development and Maintenance in White and Gray Matter Brain Regions. Front Immunol. 2019; 10: 2199.

39. Udomsinprasert W, Jittikoon J, Honsawek S. Interleukin-34 as a promising clinical biomarker and therapeutic target for inflammatory arthritis. Cytokine Growth Factor Rev. 2019; 47: 43–53.

40. van Eegher S, Perez-Lozano M-L, Toillon I, et al. The differentiation of prehypertrophic into hypertrophic chondrocytes drives an OA-remodeling program and IL-34 expression. Osteoarthritis Cartilage. 2021; 29: 257–68.

41. Salie R, Kneissel M, Vukevic M, et al. Ubiquitous overexpression of Hey1 transcription factor leads to osteopenia and chondrocyte hypertrophy in bone. Bone. 2010; 46: 680–94.

42. Sgariglia F, Candela ME, Huegel J, et al. Epiphyseal abnormalities, trabecular bone loss and articular chondrocyte hypertrophy develop in the long bones of postnatal Ext1-deficient mice. Bone. 2013; 57: 220–31.

43. Gartland A, Mason-Savas A, Yang M, MacKay CA, Birnbaum MJ, Odgren PR. Septoclast deficiency accompanies postnatal growth plate chondrodysplasia in the toothless (tl) osteopetrotic, colony-stimulating factor-1 (CSF-1)-deficient rat and is partially responsive to CSF-1 injections. Am J Pathol. 2009; 175: 2668–75.

44. Sanchez CP, He Y-Z. Bone growth during rapamycin therapy in young rats. BMC Pediatr. 2009; 9: 3.

45. Usmani SE, Pest MA, Kim G, Ohora SN, Qin L, Beier F. Transforming growth factor alpha controls the transition from hypertrophic cartilage to bone during endochondral bone growth. Bone. 2012; 51: 131–41.

46. Lézot F, Chesneau J, Navet B, et al. Skeletal consequences of RANKL-blocking antibody (IK22-5) injections during growth: mouse strain disparities and synergic effect with zoledronic acid. Bone. 2015; 73: 51–9.

47. Rashid H, Smith CM, Convers V, Clark K, Javed A. Runx2 deletion in hypertrophic chondrocytes impairs osteoclast mediated bone resorption. Bone. 2024; 181: 117014.

48. Steffey CL. Pediatric Osteoporosis. Pediatr Rev. 2019; 40: 259–61.

49. Stark Z, Savarirayan R. Osteopetrosis. Orphanet J Rare Dis. 2009; 4: 5.

50. Cohen MM. The new bone biology: pathologic, molecular, and clinical correlates. Am J Med Genet A. 2006; 140: 2646–706.

51. Atkins GJ, Kostakis P, Pan B, et al. RANKL expression is related to the differentiation state of human osteoblasts. J Bone Miner Res. 2003; 18: 1088–98.

52. Galli C, Fu Q, Wang W, et al. Commitment to the osteoblast lineage is not required for RANKL gene expression. J Biol Chem. 2009; 284: 12654–62.

53. Chemel M, Brion R, Segaliny A-I, et al. Bone Morphogenetic Protein 2 and Transforming Growth Factor β1 Inhibit the Expression of the Proinflammatory Cytokine IL-34 in Rheumatoid Arthritis Synovial Fibroblasts. Am J Pathol. 2017; 187: 156–62.

54. Wang M, Min HS, Shan H, et al. Bone morphogenetic protein 2 controls steroid-induced osteonecrosis of the femoral head via directly inhibiting interleukin-34 expression. J Mol Endocrinol. 2021; 68: 1–9.

55. Chae D-S, Han S, Lee M-K, Kim S-W. BMP-2 Genome-Edited Human MSCs Protect against Cartilage Degeneration via Suppression of IL-34 in Collagen-Induced Arthritis. Int J Mol Sci. 2023; 24: 8223.

56. Baghdadi M, Endo H, Tanaka Y, Wada H, Seino K-I. Interleukin 34, from pathogenesis to clinical applications. Cytokine. 2017; 99: 139–47.

57. Franzè E, Stolfi C, Troncone E, Scarozza P, Monteleone G. Role of Interleukin-34 in Cancer. Cancers (Basel). 2020; 12: 252.

58. Monteleone G, Franzè E, Maresca C, Colella M, Pacifico T, Stolfi C. Targeted Therapy of Interleukin-34 as a Promising Approach to Overcome Cancer Therapy Resistance. Cancers (Basel). 2023; 15: 971.

59. Alshaebi F, Safi M, Algabri YA, et al. Interleukin-34 and immune checkpoint inhibitors: Unified weapons against cancer. Front Oncol. 2023; 13: 1099696.

60. Hruscha A, Krawitz P, Rechenberg A, et al. Efficient CRISPR/Cas9 genome editing with low off-target effects in zebrafish. Development. 2013; 140: 4982–7.

61. Keatinge M, Tsarouchas TM, Munir T, et al. CRISPR gRNA phenotypic screening in zebrafish reveals pro-regenerative genes in spinal cord injury. PLoS Genet. 2021; 17: e1009515.

62. Rigueur D, Lyons KM. Whole-mount skeletal staining. Methods Mol Biol. 2014; 1130: 113–21.

63. Kamijo S, Nakajima A, Ikeda K, et al. Amelioration of bone loss in collagen-induced arthritis by neutralizing anti-RANKL monoclonal antibody. Biochem Biophys Res Commun. 2006; 347: 124–32.

64. Vargas-Franco JW, Castaneda B, Gama A, et al. Genetically-achieved disturbances to the expression levels of TNFSF11 receptors modulate the effects of zoledronic acid on growing mouse skeletons. Biochem Pharmacol. 2019; 168: 133–48.

65. Lézot F, Chesneau J, Battaglia S, et al. Preclinical evidence of potential craniofacial adverse effect of zoledronic acid in pediatric patients with bone malignancies. Bone. 2014; 68: 146–52.

66. Lézot F, Thomas BL, Blin-Wakkach C, et al. Dlx homeobox gene family expression in osteoclasts. J Cell Physiol. 2010; 223: 779–87.

67. Gobin B, Huin MB, Lamoureux F, et al. BYL719, a new α-specific PI3K inhibitor: single administration and in combination with conventional chemotherapy for the treatment of osteosarcoma. Int J Cancer. 2015; 136: 784–96.

68. Téletchéa S, Stresing V, Hervouet S, et al. Novel RANK antagonists for the treatment of bone-resorptive disease: theoretical predictions and experimental validation. J Bone Miner Res. 2014; 29: 1466–77.

69. Lamoureux F, Baud'huin M, Rodriguez Calleja L, et al. Selective inhibition of BET bromodomain epigenetic signalling interferes with the bone-associated tumour vicious cycle. Nat Commun. 2014; 5: 3511.

70. Madel M-B, Halper J, Ibáñez L, et al. Specific targeting of inflammatory osteoclastogenesis by the probiotic yeast S. boulardii CNCM I-745 reduces bone loss in osteoporosis. Elife. 2023; 12: e82037.

71. Keller S, Nickel J, Zhang J-L, Sebald W, Mueller TD. Molecular recognition of BMP-2 and BMP receptor IA. Nat Struct Mol Biol. 2004; 11: 481–8.

72. Felix J, De Munck S, Verstraete K, et al. Structure and Assembly Mechanism of the Signaling Complex Mediated by Human CSF-1. Structure. 2015; 23: 1621–31.

73. Ma X, Lin WY, Chen Y, et al. Structural basis for the dual recognition of helical cytokines IL-34 and CSF-1 by CSF-1R. Structure. 2012; 20: 676–87.

74. Kozakov D, Hall DR, Xia B, et al. The ClusPro web server for protein-protein docking. Nat Protoc. 2017; 12: 255–78.

75. Krissinel E, Henrick K. Inference of macromolecular assemblies from crystalline state. J Mol Biol. 2007; 372: 774–97.

76. Nickel J, Dreyer MK, Kirsch T, Sebald W. The crystal structure of the BMP-2:BMPR-IA complex and the generation of BMP-2 antagonists. J Bone Joint Surg Am. 2001; 83-A Suppl 1: S7-14.

77. Knaus P, Sebald W. Cooperativity of binding epitopes and receptor chains in the BMP/TGFbeta superfamily. Biol Chem. 2001; 382: 1189–95.

78. Foucher ED, Blanchard S, Preisser L, et al. IL-34 Induces the Differentiation of Human Monocytes into Immunosuppressive Macrophages. Antagonistic Effects of GM-CSF and IFN?? PLoS ONE. 2013; 8.

79. Wang Y, Bugatti M, Ulland TK, Vermi W, Gilfillan S, Colonna M. Nonredundant roles of keratinocyte-derived IL-34 and neutrophil-derived CSF1 in Langerhans cell renewal in the steady state and during inflammation. Eur J Immunol. 2016; 46: 552–9.

80. Kirsch T, Sebald W, Dreyer MK. Crystal structure of the BMP-2-BRIA ectodomain complex. Nat Struct Biol. 2000; 7: 492–6.

81. Allendorph GP, Vale WW, Choe S. Structure of the ternary signaling complex of a TGF-beta superfamily member. Proc Natl Acad Sci U S A. 2006; 103: 7643–8.

82. Healey EG, Bishop B, Elegheert J, Bell CH, Padilla-Parra S, Siebold C. Repulsive guidance molecule is a structural bridge between neogenin and bone morphogenetic protein. Nat Struct Mol Biol. 2015; 22: 458–65.

83. Robert C, Kerff F, Bouillenne F, et al. Structural analysis of the interaction between human cytokine BMP-2 and the antagonist Noggin reveals molecular details of cell chondrogenesis inhibition. J Biol Chem. 2023; 299: 102892.

84. Allendorph GP, Isaacs MJ, Kawakami Y, Izpisua Belmonte JC, Choe S. BMP-3 and BMP-6 structures illuminate the nature of binding specificity with receptors. Biochemistry. 2007; 46: 12238–47.

85. Saremba S, Nickel J, Seher A, Kotzsch A, Sebald W, Mueller TD. Type I receptor binding of bone morphogenetic protein 6 is dependent on N-glycosylation of the ligand. FEBS J. 2008; 275: 172–83.

86. Griffith DL, Keck PC, Sampath TK, Rueger DC, Carlson WD. Three-dimensional structure of recombinant human osteogenic protein 1: structural paradigm for the transforming growth factor beta superfamily. Proc Natl Acad Sci U S A. 1996; 93: 878–83.

Figure 1

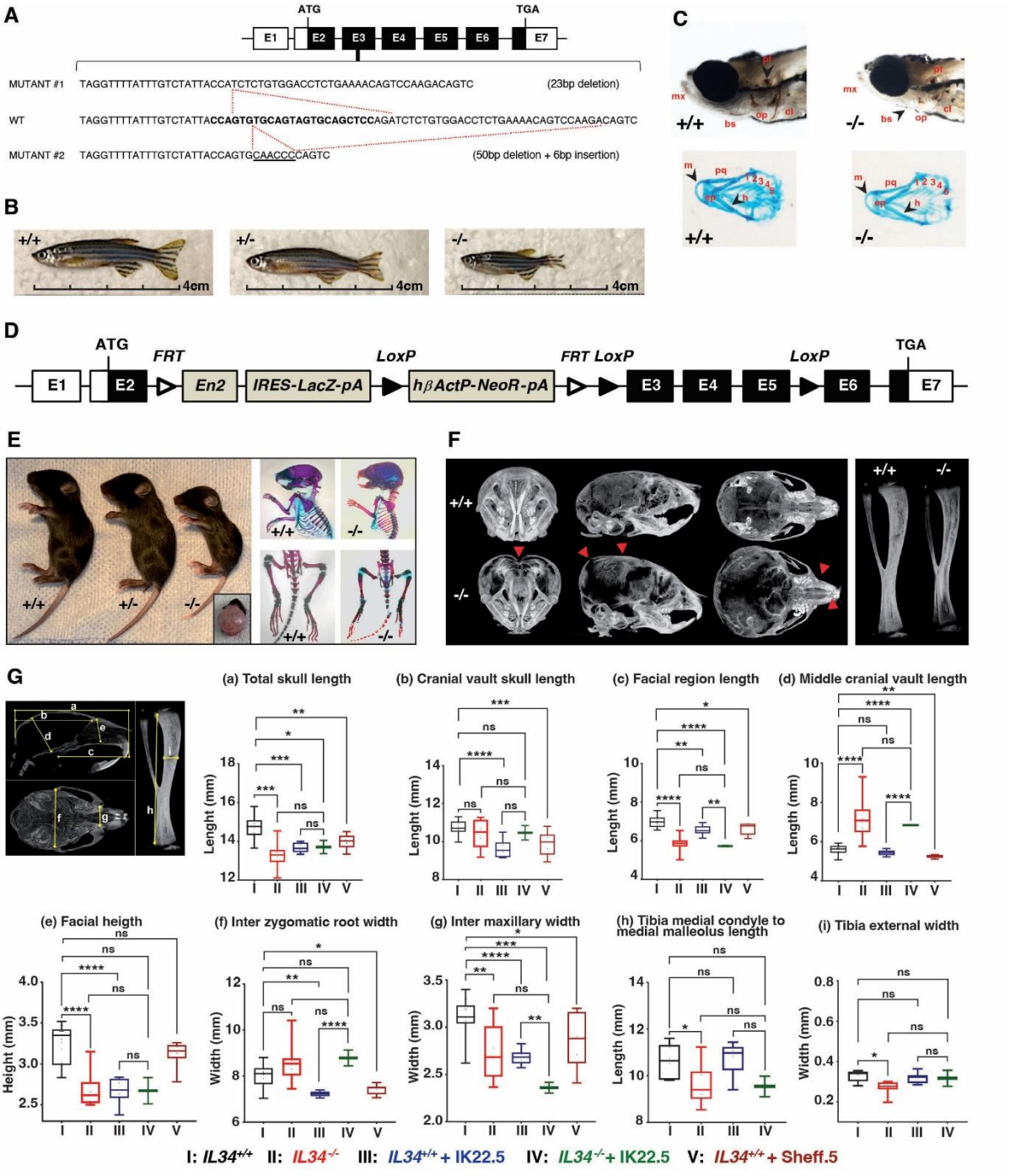

Figure 1. Growth alterations associated with *IL34* genetic invalidations in zebrafish and mouse. (**A**) Scheme of IL34 Exon3 genetic alterations induced by CrispR/Cas9 technology in zebrafish. (**B**) Images of zebrafish mutants compared to the control at age of 3 months. (**C**) Mineralization of craniofacial skeleton by Von Kossa and Acian Blue staining of embryos at 5 days post fecundation. Abbreviations: mx - branchio maxilla, bs - branchistegal ray, op - opercle, cl - cleithrum, pt - pharyngeal teeth, m - Meckel's cartilage, pq - palatoquadrate, ch - ceratohyal, ep - ethmoid plate, marked 1-5 - different arches. (**D**) Scheme of *Il34* floxed allele used to obtain constitutive invalidation of *IL34* in mouse by removing exons 3 to 5 under CRE recombinase activity. (**E**) Images at 15 days after birth of consequences of the constitutive invalidation of *IL34* with detail of hydrocephaly in *Il34*$^{-/-}$ mouse (left panel). And comparative of skeletons at 15 postnatal days visualized by Alizarin red / Alcian blue double staining (right panel). (**F**) MicroCT scan 3D reconstructions of skull and tibia enable to visualize growth defects (red arrowheads). (**G**) Quantification of growth defects in the different morphometric planes (a to i) in wile type (black box) *vs.* *Il34*$^{-/-}$ mice (red box), both treated with

IK22.5 RANKL blocking antibody (blue and green boxes), or wile type mice with Sheff.5 IL34 blocking antibody (brown box). *p<0.05, **p<0.01, ***p<0.001, ****p<0.0001**.** The differences between the experimental conditions were assessed one-way ANOVA test. n=8 except for *Il34*$^{-/-}$ + IK22.5 (n=4).

Figure 2

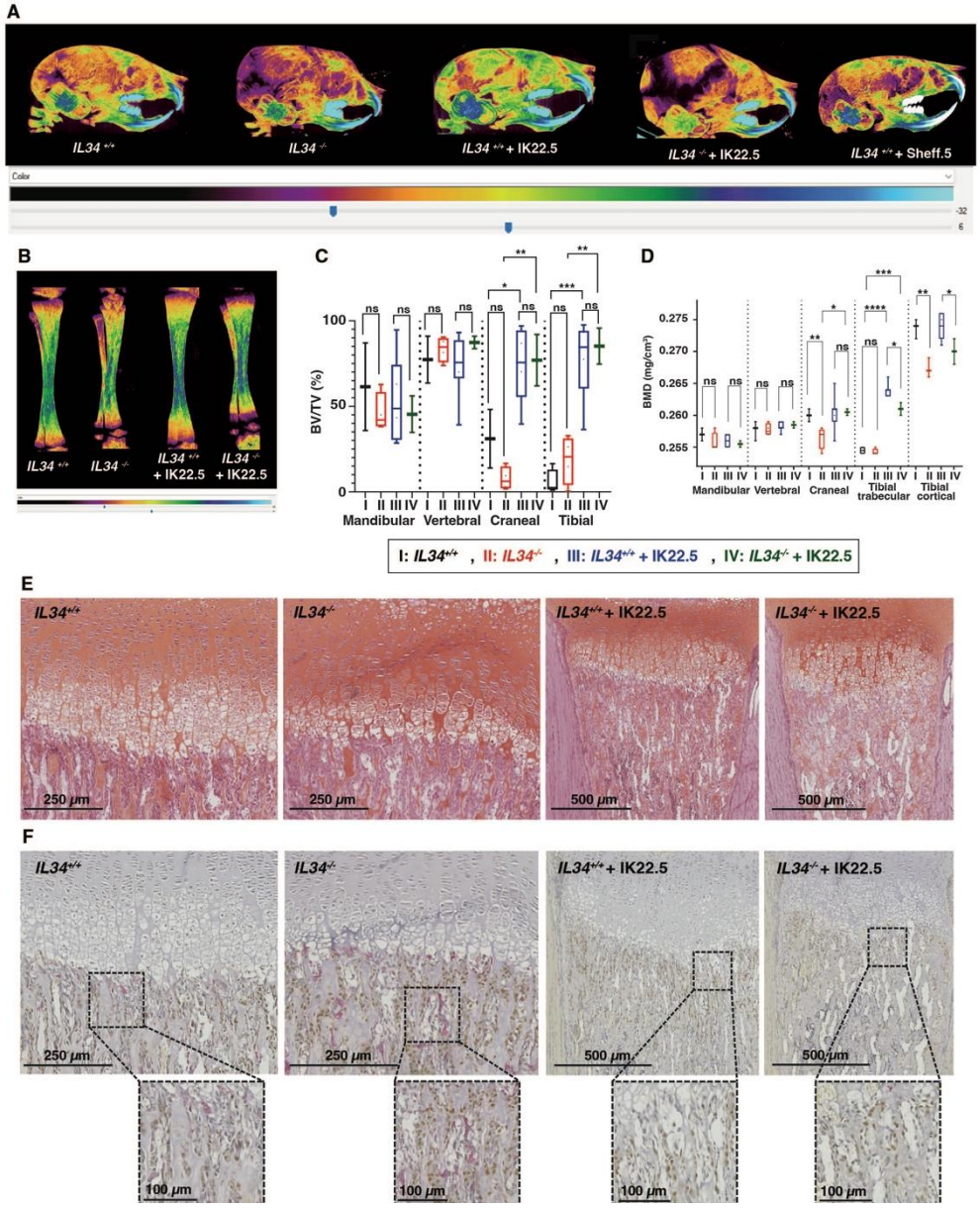

Figure 2. Bone mineral and histologic alterations associated with *IL34* genetic invalidation in mouse. (**A**) Comparative analyses of skull bones mineralization levels between *Il34*$^{+/+}$, *Il34*$^{-/-}$, *Il34*$^{+/+}$ injected with IK22.5 antibody, *Il34*$^{-/-}$ injected with IK22.5 antibody and *Il34*$^{+/+}$ injected with Sheff.5 antibody mice at age of 15 days, using profile views of the microCT scan 3D reconstructions. The color density ranges from black (lower mineralization) to clear blue (higher mineralization). (**B**) Comparative analyses of tibias mineralization levels between *Il34*$^{+/+}$, *Il34*$^{-/-}$, *Il34*$^{+/+}$ treated with IK22.5 antibody and *Il34*$^{-/-}$ treated with IK22.5 antibody mice at age of 15 days, using longitudinal views of the microCT scan 3D reconstructions. (**C**) Comparative analysis of the bone volume (BV)/total volume (TV) ratio between *Il34*$^{+/+}$, *Il34*$^{-/-}$, *Il34*$^{+/+}$ treated with IK22.5 antibody and *Il34*$^{-/-}$ treated with IK22.5 antibody in bone of different anatomical sites: the mandible, the vertebra, the skull and the tibia. *p<0.05, **p<0.01, ***p<0.001, ****p<0.0001, ns: not significant. n=8 except for *Il34*$^{-/-}$ + IK22.5 (n=4). (**D**) Comparative analysis of the bone mineral density (BMD) between *Il34*$^{+/+}$, *Il34*$^{-/-}$, *Il34*$^{+/+}$ treated with IK22.5 antibody and *Il34*$^{-/-}$ treated with IK22.5 antibody in bone of different anatomical sites: the mandible, the

vertebra, the skull and the tibia. Two areas were considered for the tibia, the trabecular and the cortical. *p<0.05, **p<0.01, ***p<0.001, ****p<0.0001, ns: not significant. n=8 except for *Il34*$^{-/-}$ + IK22.5 (n=4). (**E**) Chondrocytes stained by safranin-O staining of tibia longitudinal sections at the level of the proximal epiphysis performed for *Il34*$^{-/-}$ and *Il34*$^{+/+}$ mice injected or not with the IK22.5 antibody. (**F**) Tartrate resistant acid phosphatase (TRAP) and Osterix (Osx/SP7) dual-staining of tibia longitudinal sections at the level of the proximal epiphysis performed for *Il34*$^{-/-}$ and *Il34*$^{+/+}$ mice injected or not with the IK22.5 antibody. TRAP red staining for osteoclast cells. OSX brown staining for pre-osteoblasts cells. The scales are given as bars with the corresponding values in the lower part of each histological view.

Figure 3

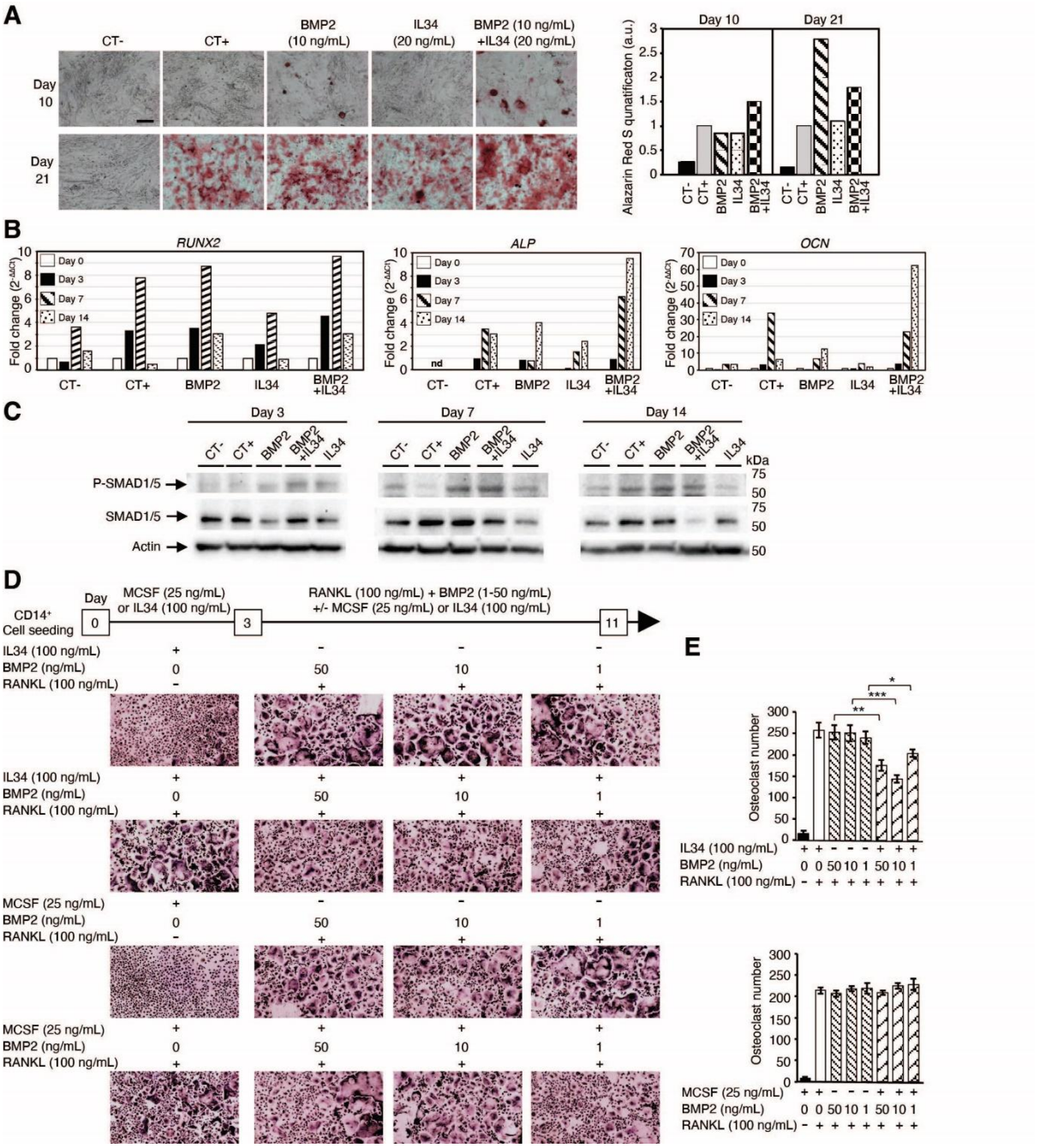

Figure 3. IL34 regulates BMP2-associated osteoblastic and osteoclastic differentiation. (**A**) Images of human mesenchymal stem cells differentiated into osteoblasts cultured in basic culture medium (CT-) or in osteogenic culture medium (CT+) in the absence or presence of BMP2 (10 ng/mL), IL34 (20 ng/mL) or combination of both at 10 and 21 days. Right panel: quantification of alizarin red staining. Magnification was similar for all views and the bar in CT- view at day 10 corresponds to 500 µm. (**B**) Real-time PCR quantification of early (*RUNX2*) and late (*ALP* and *OCN*) markers of osteoblastogenesis at days 0, 3 7 and 14. Data correspond to fold increase by $2^{-\Delta\Delta Ct}$ (cycle threshold) method. A representative experiment is shown. nd: non detected. (**C**) Western blot analysis of SMDA1/5 phosphorylation at different times of human mesenchymal stem cells differentiated into osteoblasts in basic culture medium (CT-) and in osteogenic culture medium (CT+) in the absence or presence of BMP2 (10 ng/mL), IL34 (20 ng/mL) or combination of both. (**D**) Differentiation of human $CD14^+$ cells into osteoclastic cells analyzed by Tartrate Resistant Acid phosphatase activity (TRAP histoenzymology: purple staining) after 3-day culture period in the presence of MCSF (25 ng/mL) or IL34 (100 ng/mL), followed by an 8-day period of maturation with the addition of RANKL (100 ng/mL) and /or BMP2

addition (concentrations from 1 to 50 ng/mL) (**E**) Quantification of the different experiments repeated in triplicate and presented in **D**. At least two independent experiments have been carried in triplicate. *p<0.05, **p<0.01, ***p<0.001.

Figure 4

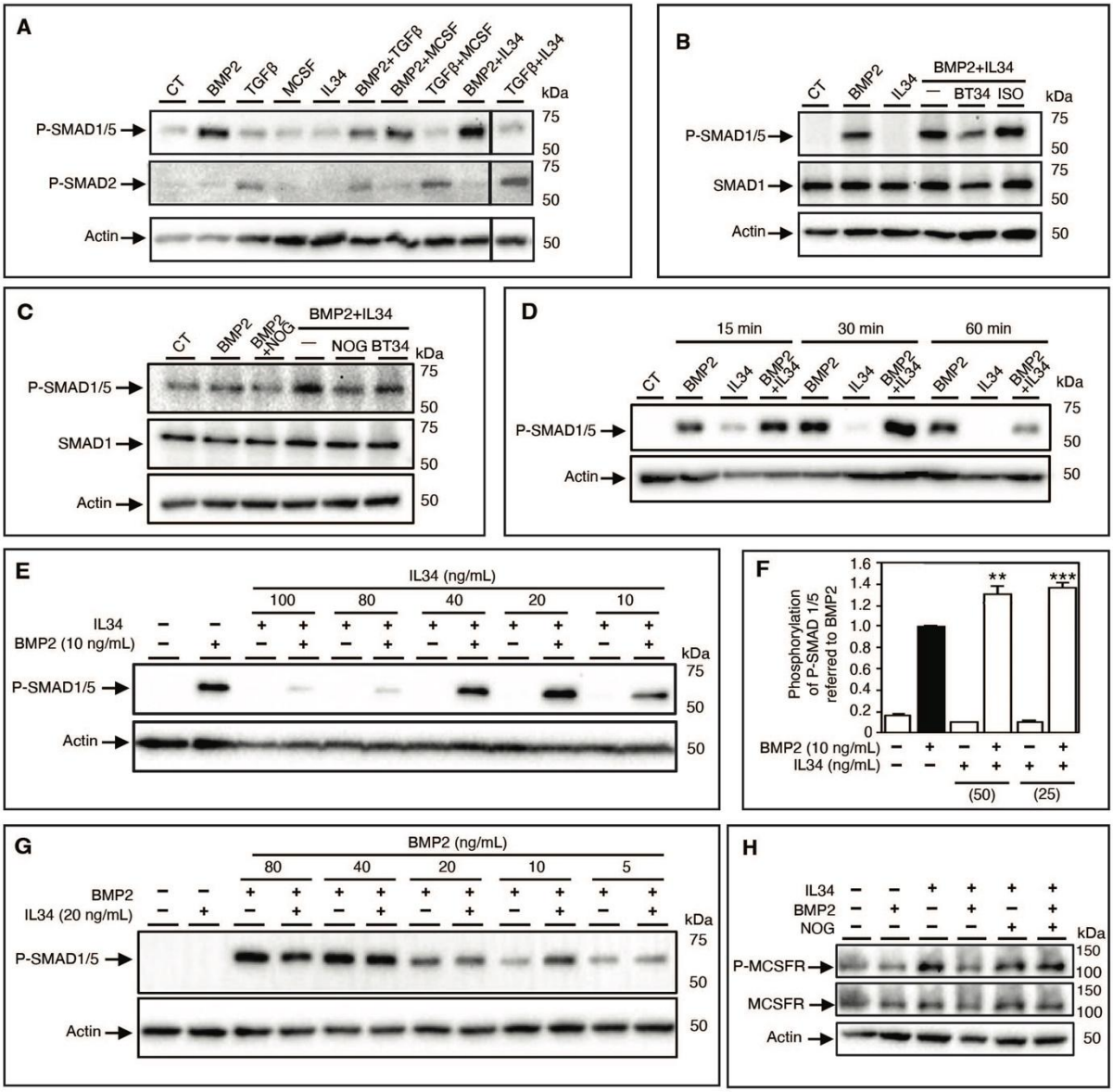

Figure 4. The interaction IL34-BMP2 modulates SMAD1/5 as well as MCSF receptor (MCSFR) phosphorylation and related signaling. (A) Western blot analysis of SMDA1/5 and SMAD2 phosphorylations of human MNNG-HOS osteosarcoma cells in the presence of BMP2 (10 ng/mL), TGFß (10 ng/mL), MCSF (20 ng/mL), IL34 (20 ng/mL) alone or in corresponding combination. A representative experiment is shown. CT: basic culture medium. (B) Western blot analysis of SMDA1/5 phosphorylation of human MNNG-HOS osteosarcoma cells in the presence of BMP2 (10 ng/mL), IL34 (20 ng/mL) alone or in combination (BMP2+IL34, -) plus the human IL34 blocking antibody (BT34) (100 µg/mL) or its irrelevant isotypic control antibody (ISO) (100 µg/mL). CT: basic culture medium. (C) Western blot analysis of SMDA1/5, similar conditions used in B in the presence of the human IL34 blocking antibody (BT34) (100 µg/mL) or the natural inhibitor of BMP2 called NOGGIN (NOG) (200 ng/mL). (D) Kinetic analysis by Western blot of the potentiating effect of IL34 on BMP2-induced SMAD1/5 phosphorylation at 15 min, 30 min and 60 min with similar corresponding molecules concentrations described in B. (E) Western blot analysis of SMDA1/5 as described in B in the presence of a single concentration of BMP2 (10 ng/mL) in combination with gradual quantities of IL34 (10, 20, 40, 80 and 100 ng/mL). (F) The Alpha SureFire technology (Revvity) was used to quantitatively validate the potentiation effect of IL34 on BMP2 activation of SMAD1/5 phosphorylation. Co-additions of 25 or 50 ng/mL of IL34 increased significantly the phosphorylation of SMAD1/5 induced by the addition of BMP2 at 10 ng/mL. **p<0.01, ***p<0.001. (G) Western blot analysis of SMDA1/5 as described in B with a single concentration of IL34 (20 ng/mL) in combination with gradual quantities of IL34 (5, 10, 20, 40

and 80 ng/mL). (H) Western blot analysis of MCSFR phosphorylation expressed in HEK293 transfected cells in the presence or absence of BMP2 (10 ng/mL), IL34 (20 ng/mL) or in combination (BMP2+IL34, -) plus NOGGIN (NOG) (200 ng/mL). Quantifications of all the Western blots presented in this figure are shown in Figure S12. All experiments have done at least three times independently.

Figure 5

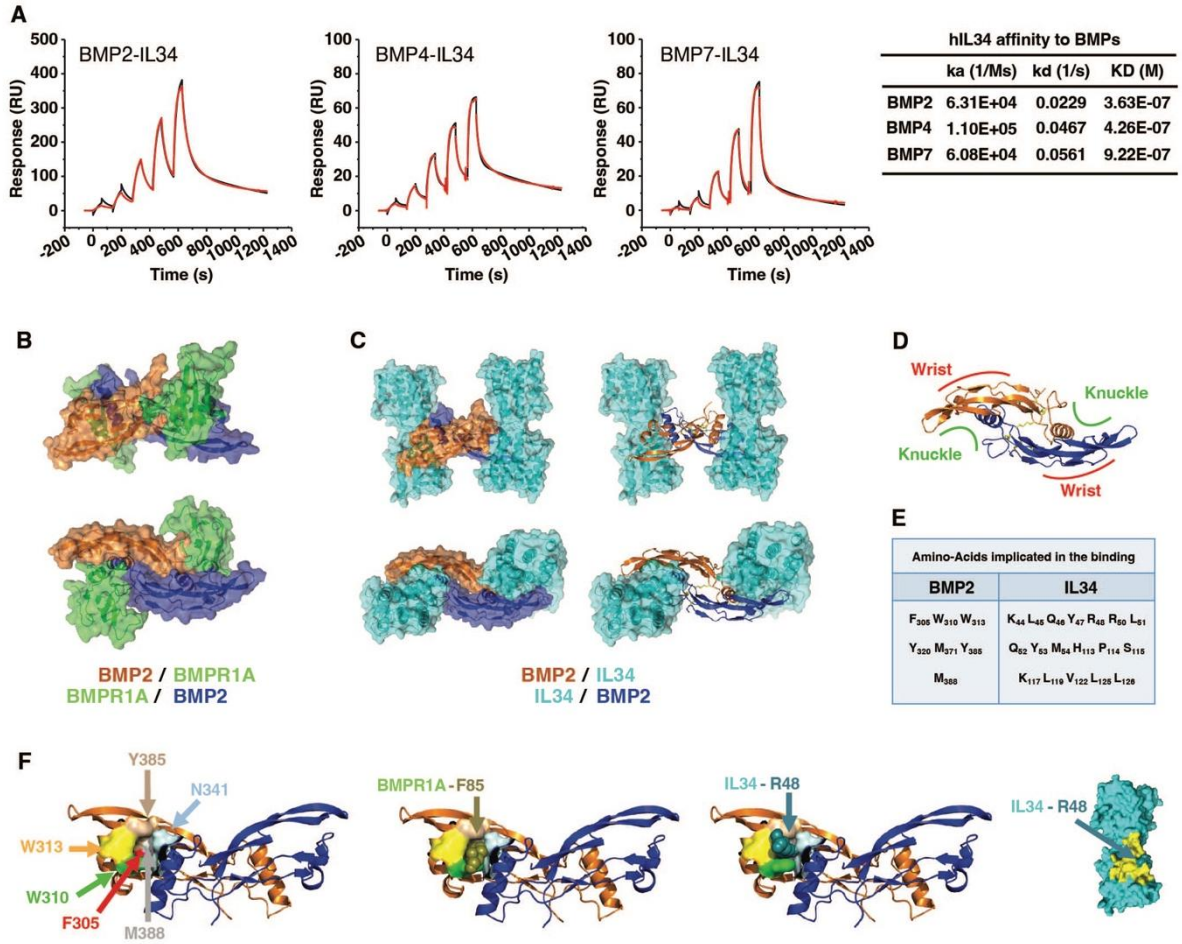

Figure 5. Demonstration and deciphering at the molecular level of the physical interaction between the IL34 protein and proteins of the BMP family. (**A**) Surface plasmon resonance experiments (described in Materials and Methods section) and values of proteins interaction parameters between IL34 and BMPs. ka: association rate constant, kd: dissociation rate constant, KD: affinity constant. (**B**) Molecular modelling of the binding of two BMPR1A receptors (green) to a BMP2 dimer (brown and dark blue) by using PyMOL. (**C**) Molecular modelling of the binding of two IL34 proteins (cyan) to a BMP2 dimer (brown and dark blue) seen in profile (top) and from above (bottom) with a representation of the BMP2 proteins in surface (left) and in structure (right) by using PyMOL. (**D**) Structural representation of a BMP2 dimer seen from above with the location of the "Knuckle" and "Wrist" binding sites to the type 1 and type 2 receptors respectively as described by Sebald and collaborators [76,77]. (**E**) Main amino acid of BMP2 and IL34 identified as being involved in binding. In addition, hydrogen bonds and salt bridges were found between BMP2 and IL34, more specifically between residues K383-D190, D312-K55 and E376-R73. (**F**) Localization on the representation of the BMP2 protein in structure of amino acids important for partner binding: F305 in red, W310 in bright green, W313 in yellow, Y385 in light brown and M388 in grey. These amino acids delineate the pocket in which residues F85 of BMPR1A and R48 of IL34 are positioned during their interaction with BMP2. The amino acid N341 presented in light blue, despite is localization in the most outside part of the pocket, was not identified as important for the binding to IL34. IL34 is displayed in surface representation with the entire binding region colored in yellow, and the important intercalating residue R48 is indicated in duck blue.

Figure 6

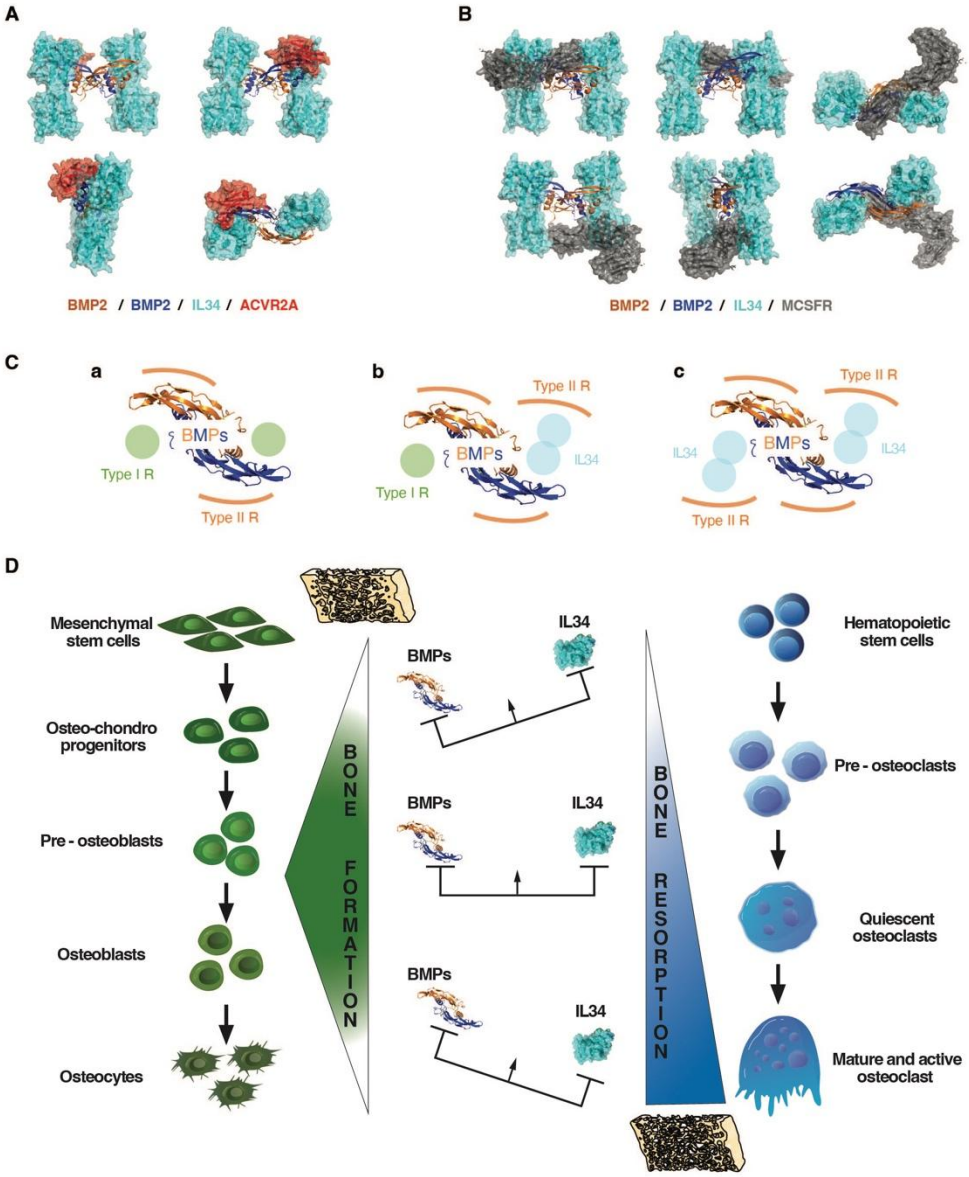

Figure 6. Impacts of the binding between BMP2 and IL34 on the ability of BMP2 and IL34 to bind to ACVR2A and MCSFR receptors respectively: importance of stoichiometry and functional consequences on bone formation and resorption. (**A**) ACVR2A receptor binding to BMP2 ("Wrist" site) does not appear to be affected by IL34 binding to the "Knuckle" sites of a BMP2 dimer. (**B**) MCSFR receptor binding to IL34 occurs at a site overlapping the BMP2 "Knuckle" site binding site. Simultaneous binding of BMP2 and MCSFR to IL34 is therefore impossible. (**C**) BMP receptor binding stoichiometry to a BMP2 dimer. The standard binding of two type 1 and two type 2 receptors per dimer (a), is gradually modified by the amount of IL34 present with potential transformation of a "Knuckle" site into a "Wrist"-like site at intermediate concentrations (b), then a second at high IL34 concentrations (c), bearing in mind that IL34 can bind type 2 BMP receptors. (**D**) Schematic representation of the impact of different ratios of BMPs and IL34 on bone formation and resorption.

Supplementary Figure Legends

Figure S1. Tools to *IL34* genetic invalidation in zebrafish using CrispR/Cas9 technology and functional confirmation. (**A**) Schematic representation of the targeted sequence in *il34* exon 3 including the protospacer adjacent motif (PAM) and the use guide RNA template sequence containing a T7 promoter sequence and the reverse targeted sequence and PAM. (**B-E)** Functional confirmation of *il34* invalidation was achieved showing the loss of the known IL34 effects on the differentiation and survival of monocytes and macrophages, [6,78] using the caudal fin amputations strategy on 3 day embryos from a heterozygous (+/-) in-cross of the double transgenic line *tg*(fms: GFP). This line contained the heterozygous mutant *il34* allele, and GFP expression of macrophages was driven by the *MCSFR* promoter. To visualize these inflammatory cells throughout injury, live images of the amputated caudal fins were taken at 8 hours post fin injuries. The 8 hours-time-point was chosen as this is the optimal time for recruitment of macrophages to the site of injury. At this time, despite no variation of *MCSF* and *MCSFR* transcript expression levels induced by IL34 invalidation **B-C**, an important reduction of the number of macrophages recruited **D-E** was observed in the $il34^{-/-}$ comparatively to the control ($il34^{+/+}$).

Figure S2. *IL34* genetic invalidation in mouse. $Il34^{Flox}$ allele (Genbank: JN962093.1) and the derived $Il34^{LacZ}$ allele obtained after recombination between its 5' and 3' LoxP sites are graphically represented. Primers used to genotype the different alleles are given in the table and positioned on the different graphical representations. Primers S3 and AS2 enable to discriminate the $Il34^{Flox}$ allele from the WT allele with respectively amplification of 240 bp and 290 bp fragments. Primers S2 and AS2 enable to identify the $Il34^{LacZ}$ allele corresponding to the amplification of a 440 bp fragment. LacZ and NeoR primer pairs were used to check the integrity of the $Il34^{Flox}$ allele. Fragments amplified with S1-AS1 and S2-AS2 primer pairs from genomic DNA extracted from $Il34^{LacZ/LacZ}$ mouse tail were Sanger sequenced to confirm recombination terminals (sequences corresponding to the construct cassette are underlined). The disruption of IL34 has been also analyzed by western blot. Briefly, whole protein extracts were obtained from frozen spleens from WT and IL34 null mice and specific antibody targeting IL34 was used. As showed, IL34 was only detected in WT and not in IL34 null sample.

Figure S3. Functional confirmation of *IL34* invalidation and *IL34 LacZ* reporter in mouse. (**A-D**) In order to confirm the effective loss of IL34 function in $Il34^{-/-}$ mouse, skin well-known as an IL34 expression site [25] was used. Correlated to IL34 invalidation, a significant reduction of CD207 expressing cell (Langerhans cells) was observed. (**E**) ß-galactosidase staining (blue) performed on section of $Il34^{+/LacZ}$ mouse enable to confirm previously described expression of IL34 [24,25,79] in some keratinocytes and cells from the hair follicle.

Figure S4. Graphical representation of morphometric parameters used for mouse head and tibia analyses, blocking antibodies injections protocol and results of bone trabecular structure analyses at different anatomical sites. (**A**) The seven morphometric parameters (a-g) measured for the head (craniofacial skeleton) and the two parameters (h-i) measured for tibia (appendicular skeleton) are listed and represented on 2D microCT scan views. (**B**) The blocking antibodies (IK22.5 and Sheff5) injections protocol was characterized by four subcutaneous injections at postnatal days 1, 3, 5 and 7 of 25 mg/kg of antibody following by a sacrifice at day 15. (**C**) The trabecular thickness (Tb. Th), the trabecular space (Tb. Sp) and the trabecular number (Tb. N) were determined at four anatomical sites, the mandible, the vertebra (C2) the skull and the tibia. $Il34^{+/+}$ are represented in black, $Il34^{-/-}$ in red, $Il34^{+/+}$ treated with IK22.5 in blue, and $Il34^{-/-}$ treated with IK22.5 in green. *p<0.05, **p<0.01, ***p<0.001, ****p<0.0001, ns: not significant. n=8 except for $Il34^{-/-}$ + IK22.5 (n=4).

Figure S5. Analyses of the impact of Sheff.5 antibody injections in WT pups on the bone trabecular structure (Tb. Th, Tb. Sp and Tb. N), the percentage of BV/TV and BMD. No significant variation was observed comparatively to pups injected with a control irrelevant antibody from the same idiotype whatever the parameter considered. ns: not significant. CT: control group. n=8.

Figure S6. Histological comparative analysis of the tibia proximal epiphysis area of 15-day-old $Il34^{-/-}$ and $Il34^{+/+}$ mice using Masson's trichome stained longitudinal sections. An important reduction of the thickness of the hypertrophic chondrocytes area was observed in the null mutant. The scales are given as bars with the corresponding values in the lower part of each histological view.

Figure S7. High magnification views of tartrate resistant acid phosphatase (TRAP) and Osterix dual-staining of tibia longitudinal sections at the level of the proximal epiphysis performed for 15-day-old *Il34*$^{-/-}$ and *Il34*$^{+/+}$ mice treated or not with the IK22.5 antibody. An important increase of both staining (TRAP in red and OSX in brown) was observed in the null mutant mouse. The IK22.5 injections drastically reduced the number of TRAP-positive cells in both *Il34*$^{-/-}$ and *Il34*$^{+/+}$ mice, whereas no evident variation of the number of cells stained for OSX was evidenced. The scale is given as a bar corresponding to 50 μm in the lower part of each histological view.

Figure S8. Comparative analysis of RUNX2 expression in the tibia proximal epiphysis area of 15-day-old *Il34*$^{-/-}$ and *Il34*$^{+/+}$ mice treated or not with the IK22.5 antibody using immunohistochemistry applied to longitudinal sections. No variation of the number of stained cells was evidenced between *Il34*$^{-/-}$ and *Il34*$^{+/+}$ mice as between *Il34*$^{-/-}$ and *Il34*$^{+/+}$ injected with IK22.5 antibody. The scale is given as a bar corresponding to 250 μm in the lower part of each histological view.

Figure S9. Functional impact of BMP2, IL34 or combined BMP2+IL34 addition in the culture medium onto osteoblastic differentiations. (**A**) BMP2 addition (10 ng/mL) to the osteogenic differentiation medium (CT+) induced an acceleration of the differentiation as evidenced by the higher alizarin red staining corresponding to phosphocalcic crystal deposition at 7, 14 and 21 days. IL34 addition (20 ng/mL) to the osteogenic differentiation medium had no effect on the differentiation (view not shown but the quantification is presented in **B**, right panel). Co-addition of IL34 (10, 20 or 40 ng/mL) with BMP2 (10 ng/mL) potentialized the acceleration of the osteoblastic differentiation observed with BMP2 alone with an optimal concentration ratio (ng/mL) of 2 between BMP2 and IL34. Magnification is similar for all views and the bar in CT- view at day 7 correspond to 500 μm. (**B**) Quantification of the alizarin red staining corresponding to independent experiments from different donors. BIL: BMP2+IL34 addition; Numbers (10, 20 or 40) correspond to the used concentrations of IL34 in ng/mL.

Figure S10. Impacts of the additions of BMP2 (10 ng/mL), IL34 (20 ng/mL) or BMP2+IL34 to the CT+ medium onto the expression of early (*RUNX2*) and late (*ALP* and *OCN*) markers of osteoblast differentiation, onto osteoprotegerin (*OPG*, a major regulatory factor of osteoclastogenesis), and onto type 1 and type 2 receptors of the BMPs (*BMPR1A*, *BMPR2* and *ACVR2A*). Results of three different experiments (Exp. 1 to 3) carried out with three different batches of mesenchymal stem cells (obtained from different donors) are presented in order to deal with the inter-batches variabilities considering only results similarly observed in the three experiments. BMP2 addition accelerated the osteoblastic differentiation and the co-addition of IL34 potentialized this effect as evidenced for *RUNX2* expression at days 3 and 7, and for *ALP* and *OCN* at day 14. BMP2 addition alone or in combination with IL34 reduced the *OPG* expression at days 3 and 7. Regarding the different receptors of the BMPs, no reproducible effects were observed between experiments, but all three receptors are expressed at all stages (days) of differentiation whatever the culture conditions used. nd: not detected.

Figure S11. Impacts of addition of different combinations of BMP4+IL34 or BMP7+IL34 onto the activation of BMP receptors evidenced by SMAD1-5 phosphorylation in human MNNG-HOS osteosarcoma cell line. (**A**) Correspondence table between concentrations used in ng/mL and in pM or nM for IL34, BMP2, BMP4 and BMP7. (**B**) Joint addition of BMP4 (graded concentrations from 5 to 80 ng/mL) and IL34 (20 ng/mL) induced SMAD1-5 phosphorylation, with greater effects observed with 20 and 80 ng/mL BMP4. (**C**) Joint addition of BMP4 (20 ng/mL) and IL34 (graded concentration from 10 to 80 ng/mL) induced SMAD1-5 phosphorylation, with an optimal effect observed with 20 ng/mL IL34. (**D**) Joint addition of BMP7 (graded concentrations from 5 to 80 ng/mL) and IL34 (20 ng/mL) induced SMAD1-5 phosphorylation, with greater effects observed with 10 and 80 ng/mL BMP7. (**E**) Joint addition of BMP7 (10 ng/mL) and IL34 (graded concentration from 10 to 80 ng/mL) induces SMAD1-5 phosphorylation, with greater effects observed with 20 and 40 ng/mL IL34.

Figure S12. Quantitative analyses of Western blots presented in Figure 4. Histograms corresponding to the control condition, the BMP2-only condition and the IL34-only condition appear in red, black and blue respectively. *p<0.05, **p<0.01.

Figure S13. Curves obtained during the surface plasmon resonance experiments with immobilization of the BMP proteins (2, 4 and 7) and additions of IL34 and NOGGIN alone or in combination. Whatever the BMP protein considered an effective binding of IL34 as NOGGIN was observed with an additive effect of the two factors.

Figure S14. Representative structures of BMP2 dimer bound proteins resolved experimentally. BMP-2 dimers are displayed in blue and orange surface. (**A**) BMPR1A structure (green) as found in PDB ID 1ES7 [80]. State that binding the knuckle site. (**B**) BMPR1A (green) and Activin Receptor IIA (red) occupy each wrist and knuckle epitopes (PDB ID 2GOO [81]). (**C**) RGMA (yellow) as found in PDB ID 4UHY [82]. State that binding the knuckle site. (**D**) NOGGIN was determined to occupy both epitopes in structure PDB ID 7AG0 [83]. Left: side view of protein complexes, right: top view of protein complexes.

Figure S15. Representative structures of the BMP2 dimer and IL34 in electrostatics surface view with the hydrophobic (white) and hydrophilic sites (red for negative patches, blue for positive patches) and identification of their respective binding sites. (**A**) Representation of the BMP2 dimer with the knuckle site pocket underlined (arrow). (**B**) BMP2 dimer and IL34 position in cartoon representation. (**C**) IL34 with the BMP2 binding site indicated by the arrow. (**D**) IL34 and BMP2 position in cartoon representation.

Figure S16. Analysis in the BMP-TGFß family of the conservation of the amino acids implicated in the binding to IL34 using COBALT alignment tool (NCBI). Alignment of the human protein sequences of the 29 BMP-TGFß family members was first given with amino acids implicated in the binding to IL34 conserved comparatively to BMP2 overlined in green, those changed by another with close physical-chemical proprieties overlined in blue and those changed by another with different physical-chemical proprieties overlined in yellow. Secondly for each BMP-TGFß family members the phylogenic conservation in mammalian (15 species) of the amino acids implicated in the binding to IL34 was analyzed and given. Finally, the phylogenic conservation of the amino acids of IL34 implicated in the binding to BMPs was also analyzed in the same 15 mammalian species and presented.

Figure S17. Representative structures of IL34 binding to different BMP proteins. IL34 is displayed in cyan surface. (**A**) IL34 binding to BMP3 structure (lime color) as found PDB ID 2QCQ [84]. (**B**) IL34 binding to BMP6 structure (wheat color) as found PDB ID 2R52 [85]. (**C**) IL34 binding to BMP7 structure (purple color) as found PDB ID 1BMP [86]. Left: side view of protein complexes, right: top view of protein complexes.

Figure S18. FACS comparative analysis of the populations of CD11b monocytic cells in both the bone marrow and the spleen of *Il34*$^{-/-}$ versus *Il34*$^{+/+}$ mice. In *Il34*$^{-/-}$ (IL34-KO) mice compared with *Il34*$^{+/+}$ (WT) mice, significant increases in the percentage of CD11b-positive cells were observed in both spleen (22.7% vs. 2.54%) and bone marrow (15.2% vs. 9.83%).

Figure S19. Demonstration at the molecular level of the physical interaction between the IL34 protein and proteins of the BMP receptor type II family. The surface plasmon resonance experiments showed that IL34 bound efficiently to BMPRII, ACTRIIA and ACTRIIB with KD values of 1.2E-07 M, 3.6E-07 M and 1.1E-07 M respectively.

Supplementary movie (S1)

Movie S1. Movie evidencing the simultaneous binding of one IL34 monomer (cyan), one BMPR1A monomer (green) and one ACVR2A monomer (red) on a dimer of BMP2 (blue and orange).